CSIAM Trans. Life Sci.
doi: 10.4208/csiam-ls.SO-2025-0016

Vol. **x**, No. x, pp. 1-34
xx 2025

A Brucellosis Model with Different Clinical Symptoms and a Time Delay Representing Incubation Period: Global Dynamics and Data Fitting

Siyu Kang[1,2,3], Rui Xu[1,2,*] and Huarong Ren[1,2,3]

[1] *Complex Systems Research Center, Shanxi University, Taiyuan 030006, P.R. China.*
[2] *Complex Systems and Data Science Key Laboratory of Ministry of Education, Shanxi University, Taiyuan 030006, P.R. China.*
[3] *School of Mathematics and Statistics, Shanxi University, Taiyuan 030006, P.R. China.*

Received 30 May 2025; Accepted 17 August 2025

Abstract. Brucellosis is a significant zoonotic disease that has a high incidence rate in sheep, particularly in the Inner Mongolia region of China. To better investigate its transmission dynamics, this paper proposes a sheep brucellosis model incorporating acute and chronic infections, a saturated incidence rate describing environmental transmission and a time delay representing the incubation period. By constructing Lyapunov functionals and using LaSalle's invariance principle, it is shown that the global dynamics of the disease is completely determined by the basic reproduction number: If $\mathcal{R}_0<1$, the brucellosis always dies out; if $\mathcal{R}_0>1$, a unique endemic equilibrium exists and is globally asymptotically stable. Using data of sheep brucellosis cases in Inner Mongolia from 2016 to 2020, unknown parameters and the basic reproduction number ($\mathcal{R}_0=1.544$) are estimated via the Markov chain Monte Carlo method. Numerical simulations show that reducing the transmission rate of acutely infected sheep while increasing the culling rate of symptomatic infected sheep is the most effective strategy to control the spread of brucellosis in Inner Mongolia. Notably, decreasing the proportion of acutely infected sheep or increasing acute-to-chronic conversion rate may lead to a significant short-term increase in chronically infected sheep.

AMS subject classifications: 34K20, 92D30
Key words: Brucellosis, chronic infection, basic reproduction number, global stability, data fitting.

1 Introduction

Brucellosis, also known as undulant fever, Mediterranean fever, or Malta fever, is a significant zoonotic infectious disease caused by bacteria of the genus Brucella [4, 33]. It has a global distribution and poses substantial threats to both public health and ani-

*Corresponding author. *Email address:* xurui@sxu.edu.cn (R. Xu)

mal health. The disease is particularly prevalent in regions such as the Middle East, the Mediterranean, Mexico, and Central America [12,29,30,34]. In China, brucellosis is classified as a Category II animal epidemic disease [8]. Although the number of outbreaks and infected animals in livestock decreased by 21.75% and 16.48% respectively in 2024, the pathogen persisted and continued to spread to the southern regions in 2025, maintaining a severe disease control situation [7,38,53]. The genus Brucella includes multiple species, among which Brucella abortus and Brucella melitensis are the primary pathogens, capable of spreading to humans through contact or consumption of contaminated animal products [42]. This study focuses on the transmission dynamics of brucellosis in sheep populations.

Brucellosis in sheep is primarily transmitted through direct contact with infected sheep or their secretions (such as aborted fetuses, amniotic fluid, and milk). It can also be spread indirectly through contaminated feed, water, or shared equipment. The incubation period of the disease is variable, usually lasting from 1 to 3 weeks, but it can sometimes be prolonged to several months or even over a year [39, 42]. Infected sheep show acute and chronic clinical symptoms. Acute infected sheep develop symptoms such as fever, abortion, and orchitis within a few weeks, which severely impact reproduction and production [41]. Chronic infected sheep, on the other hand, show more insidious symptoms such as weight loss, arthritis, or lameness, which can persist for several months or even years. Brucella infection not only compromises the health of sheep but also poses a threat to the livestock economy and public health.

Since the initial isolation of Brucella in 1886 [5], various mathematical models have been developed to study its transmission dynamics [1–3,11,13,20,27,32,36,43,44,47,48,55], but existing models still have limitations. Early studies widely used bilinear incidence to describe environmental transmission, but such models had clear limitations, as they struggled to reflect the saturation effect from bacterial concentration thresholds. To tackle this, Zhang *et al.* [46] innovatively introduced saturated incidence, which greatly boosted model authenticity and quantitatively analyzed prevention and control costs, offering key theoretical support for formulating strategies. However, this model overlooked the impact of the incubation period on brucellosis transmission. Hou and Zhang [18] attempted to represent the incubation period by introducing a time delay term. However, their research indicated that the influence of time delay on the stability of equilibria of the system was relatively limited, and it failed to consider acute and chronic infections. To address this issue, Liu *et al.* [22] further developed the susceptible-latent-acute infected-chronic infected-brucella (SLICB) model, incorporating seasonality, spatial heterogeneity, and nonlocal time delay. Their findings confirm that prolonging the incubation period and increasing the random walk rate of infected sheep can effectively prevent brucellosis from becoming endemic; moreover, considering only acute or chronic infections leads to significant deviations in the density of infected sheep and the time to reach a steady state. Notably, this model has not yet included the saturated incidence mechanism. Recently, the SEIVW$S_h I_{ah} I_{ch}$ model proposed by Liu *et al.* [23], although it systematically evaluated the effectiveness of various prevention and control measures such as vaccination,

still failed to achieve the synergistic integration of key factors like saturated incidence and acute and chronic infections. Based on the above work and actual conditions, an epidemic model incorporating a saturated incidence rate, latent period, and different clinical symptoms would more comprehensively and accurately reflect the transmission dynamics of brucellosis.

In the research of infectious disease modeling, the application of data fitting and Markov chain Monte Carlo (MCMC) methods is crucial [6, 9, 10, 35, 37]. Data fitting integrates actual data with infectious disease models, revealing the complex transmission mechanisms of diseases. The MCMC method estimates unknown parameters and basic reproduction numbers within the models through Bayesian inference. The combination of these two approaches can more accurately simulate and predict the spread dynamics of infectious diseases. In the study of brucellosis, it is quite common to use human case data for fitting [17, 21, 24, 25, 31, 40, 46, 49, 50]. There are numerous studies that combine data fitting with MCMC methods. For instance, Ma and Sun [25] fitted monthly human brucellosis cases with average temperature data in Xinjiang (2015–2020), estimating the basic reproduction number at 0.6691. They also explored impacts of control measures, reproductive traits, and temperature fluctuations on the disease's outbreak and transmission dynamics. Zhang *et al.* [49] estimated the basic reproduction number by fitting human cases in Inner Mongolia, further examining effects of precipitation, humidity, and atmospheric pressure there. Additionally, using price and infector data from Ningxia, Wang *et al.* [40] applied least squares for model fitting and proposed an optimal control strategy that maximizes farmers' profits while effectively controlling brucellosis. However, due to data acquisition challenges and transmission complexity, data fitting for animal brucellosis cases remains relatively scarce [45].

The article is organized as follows. In Section 2, we formulate a brucellosis model that incorporates latent delay, bilinear incidence, saturated incidence, as well as acute and chronic infections. In Section 3, we discuss the well-posedness of the solutions; calculate the basic reproduction number, interpret its biological significance; and analyze the existence and uniqueness of the endemic equilibrium. In Sections 4 and 5, we establish the local and global stability of the feasible equilibrium, respectively. In Section 6, we estimate unknown parameters and the basic reproduction number through data fitting using Brucellosis data from Inner Mongolia sheep spanning 2016 to 2020. In Section 7, we conduct sensitivity analysis of key parameters based on the basic reproduction number and endemic equilibrium, and assess the impact of single and combined control strategies on brucellosis prevention and control. Finally, we summarize the main findings of the current study and discuss some future research directions.

2 Model formulation

According to whether the sheep are infected with Brucella, infectious differences and the different clinical symptoms post-infection, we categorize the sheep into four compartments:

(1) Susceptible group refers to those that are not infected but are likely to be infected;
(2) Latency group refers to those who are infected with Brucella but have no symptoms yet;
(3) Acutely infected group refers to those that are in acute infection period after being infected with Brucella;
(4) Chronically infected group refers to those that are in chronic infection period after being infected with Brucella.

The numbers of the four groups at time t are denoted as $S(t), E(t), I(t)$ and $C(t)$, respectively. The concentration of Brucella in the environment at time t is represented by $B(t)$. According to the transmission process of brucellosis, the transmission diagram of five compartments is shown in Fig. 1. And the definitions of parameters are shown in Table 1.

Table 1: The descriptions of parameters in system (2.3).

Parameters	Biological meaning
Λ	The recruitment rate of the sheep population
β_I	The transmission rate from acutely infected sheep to susceptible sheep
β_C	The transmission rate from chronically infected sheep to susceptible sheep
β_B	The transmission rate from brucella to susceptible sheep
K	The half-saturation coefficient of brucella concentration
p	The proportion of acutely infected sheep among the infected sheep
$1-p$	The proportions of chronically infected sheep among the infected sheep
μ	Sheep natural elimination rate
ν	The surveillance culling rate of symptomatic infected sheep
δ	The probability that acute infected sheep become chronic infected sheep due to lack of timely treatment or management
ξ_1	The shedding rate from acutely infected sheep into the environment
ξ_2	The shedding rate from chronically infected sheep into the environment
r	The decaying rate of brucella in the environment
τ	The incubation period of brucellosis

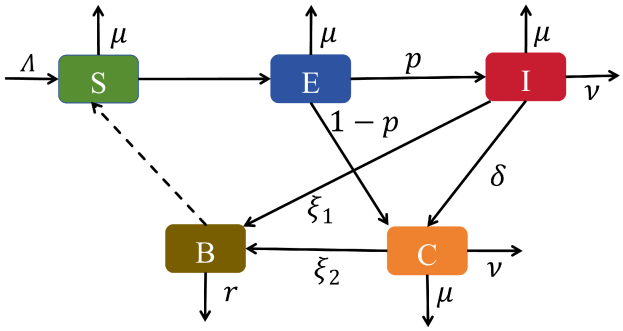

Figure 1: Transmission diagram for 5 compartments.

The following is the detailed descriptions of the changes in each compartment over time. The number of sheep added to the compartment S per unit time is Λ. Meanwhile, the number of sheep moving out of S, E, I and C per unit time due to natural death are $\mu S, \mu E, \mu I$ and μC, respectively. At time t, the total number of latent sheep newly increased due to infection is

$$N_t = \beta_I S(t) I(t) + \beta_C S(t) C(t) + \frac{\beta_B S(t) B(t)}{K + B(t)}.$$

The probability that a sheep infected at time $t-\tau$ is still alive at time t is denoted by $e^{-\mu\tau}$. Assume that the probability of an infected sheep transitioning from the latent period to the acute infection period is p, and the probability of transitioning to the chronic infection period is $1-p$. Therefore, the number of newly increased symptomatic sheep in compartment I and C at time t are

$$N_I = p e^{-\mu\tau} S(t-\tau) \left[\beta_I I(t-\tau) + \beta_C C(t-\tau) + \frac{\beta_B B(t-\tau)}{K + B(t-\tau)} \right],$$

$$N_C = (1-p) e^{-\mu\tau} S(t-\tau) \left[\beta_I I(t-\tau) + \beta_C C(t-\tau) + \frac{\beta_B B(t-\tau)}{K + B(t-\tau)} \right],$$

respectively. Due to surveillance of the symptomatic sheep, the number of sheep culled from I and C per unit time are νI and νC, respectively.

The number of sheep transferring from compartment I to C per unit time is denoted by δI. Additionally, the contribution rates of compartments I and C to Brucella concentration in the environment are $\xi_1 I(t)$ and $\xi_2 C(t)$, respectively. The concentration of Brucella in the environment decreases at rate $rB(t)$.

In the light of the transmission diagram in Fig. 1, we have the following model:

$$\begin{cases} \dot{S}(t) = \Lambda - \mu S(t) - \beta_I S(t) I(t) - \beta_C S(t) C(t) - \dfrac{\beta_B S(t) B(t)}{K + B(t)}, \\ \dot{E}(t) = \beta_I S(t) I(t) + \beta_C S(t) C(t) + \dfrac{\beta_B S(t) B(t)}{K + B(t)} - \mu E(t) \\ \qquad\quad - e^{-\mu\tau} S(t-\tau) \left[\beta_I I(t-\tau) + \beta_C C(t-\tau) + \dfrac{\beta_B B(t-\tau)}{K + B(t-\tau)} \right] \\ \dot{I}(t) = p e^{-\mu\tau} S(t-\tau) \left[\beta_I I(t-\tau) + \beta_C C(t-\tau) + \dfrac{\beta_B B(t-\tau)}{K + B(t-\tau)} \right] \\ \qquad\quad - (\mu + \nu + \delta) I(t), \\ \dot{C}(t) = (1-p) e^{-\mu\tau} S(t-\tau) \left[\beta_I I(t-\tau) + \beta_C C(t-\tau) + \dfrac{\beta_B B(t-\tau)}{K + B(t-\tau)} \right] \\ \qquad\quad + \delta I(t) - (\mu + \nu) C(t), \\ \dot{B}(t) = \xi_1 I(t) + \xi_2 C(t) - r B(t). \end{cases} \tag{2.1}$$

The initial conditions for system (2.1) take the following form:

$$\begin{aligned} &S(t)=\varphi_1(t), \quad E(t)=\varphi_2(t), \quad I(t)=\varphi_3(t), \quad C(t)=\varphi_4(t), \quad B(t)=\varphi_5(t), \\ &\varphi_i(t)\geqslant 0, \qquad t\in[-\tau,0), \qquad \varphi_i(0)>0, \qquad i=1,2,3,4,5. \end{aligned} \tag{2.2}$$

Here, $\mathbb{B}$ denotes the Banach space $C([-\tau,0],\mathbb{R}^5)$ of continuous functions mapping the interval $[-\tau,0]$ into $\mathbb{R}^5$ equipped with the sup-norm

$$\|\varphi\|=\sup_{t\in[-\tau,0]}|\varphi(t)|, \quad \phi=(\varphi_1,\varphi_2,\varphi_3,\varphi_4,\varphi_5)\in\mathbb{B}.$$

The nonnegative cone of $\mathbb{B}$ is defined as

$$\mathbb{B}^+=C([-\tau,0],\mathbb{R}^5_+), \quad \mathbb{R}^5_+=\{(\varphi_1,\varphi_2,\varphi_3,\varphi_4,\varphi_5):\varphi_i\geqslant 0, i=1,2,3,4,5\}.$$

For continuity of the initial conditions, we need to further require

$$\varphi_2(0)=\int_{-\tau}^{0}e^{\mu s}\varphi_1(s)\left[\beta_I\varphi_3(s)+\beta_C\varphi_4(s)+\frac{\beta_B\varphi_5(s)}{K+\varphi_5(s)}\right]\mathrm{d}s.$$

According to the basic theory of functional differential equations [16], it is easy to know that system (2.1) has a unique solution that satisfies the initial conditions (2.2).

Since the S,I,C and B equations in model (2.1) do not depend on variable E, it suffices to study the following system with time delay:

$$\begin{cases} \dot{S}(t)=\Lambda-\mu S(t)-\beta_I S(t)I(t)-\beta_C S(t)C(t)-\dfrac{\beta_B S(t)B(t)}{K+B(t)}, & \text{(2.3a)}\\ \dot{I}(t)=pe^{-\mu\tau}S(t-\tau)\left[\beta_I I(t-\tau)+\beta_C C(t-\tau)+\dfrac{\beta_B B(t-\tau)}{K+B(t-\tau)}\right] \\ \qquad -(\mu+\nu+\delta)I(t), & \text{(2.3b)}\\ \dot{C}(t)=(1-p)e^{-\mu\tau}S(t-\tau)\left[\beta_I I(t-\tau)+\beta_C C(t-\tau)+\dfrac{\beta_B B(t-\tau)}{K+B(t-\tau)}\right] \\ \qquad +\delta I(t)-(\mu+\nu)C(t), & \text{(2.3c)}\\ \dot{B}(t)=\xi_1 I(t)+\xi_2 C(t)-rB(t). & \text{(2.3d)} \end{cases}$$

The initial conditions for system (2.3) take the following form:

$$\begin{aligned} &S(t)=\phi_1(t), \quad I(t)=\phi_2(t), \quad C(t)=\phi_3(t), \quad B(t)=\phi_4(t), \\ &\phi_i(t)\geqslant 0, \qquad t\in[-\tau,0), \qquad \phi_i(0)>0, \qquad i=1,2,3,4., \end{aligned} \tag{2.4}$$

Here, $\mathbb{C}$ denotes the Banach space $C([-\tau,0],\mathbb{R}^4)$ of continuous functions mapping the interval $[-\tau,0]$ into $\mathbb{R}^4$ equipped with the sup-norm

$$\|\phi\|=\sup_{t\in[-\tau,0]}|\phi(t)|, \quad \phi=(\phi_1,\phi_2,\phi_3,\phi_4)\in\mathbb{C}.$$

The nonnegative cone of $\mathbb{C}$ is defined as

$$\mathbb{C}^+=C\big([-\tau,0],\mathbb{R}^4_+\big), \quad \mathbb{R}^4_+=\{(\phi_1,\phi_2,\phi_3,\phi_4):\phi_i\geqslant 0, i=1,2,3,4\}.$$

3 Preliminary results

3.1 Positivity and boundedness of solutions

In this section, we will discuss the well-posedness of the solutions to system (2.3). According to the basic theory of functional differential equations [16], it is known that system (2.3) has a unique solution that satisfies the initial conditions (2.4). Nextly, we will prove the positivity and ultimate boundedness of the solutions to system (2.3).

Theorem 3.1. *For $t\geqslant 0$, the solution of system* (2.3) *with the initial conditions* (2.4) *is positive.*

Proof. Firstly, we prove that $S(t)$ is positive for all $t\geqslant 0$. Assume the contrary and let $t_1>0$ be the first time such that $S(t_1)=0$. Then from the Eq. (2.3a), we have $\dot{S}(t_1)=\Lambda>0$, which indicates that $S(t)<0$ for $t\in(t_1-\epsilon_1,t_1)$, where ϵ_1 is an arbitrarily small positive constant. This contradicts with the fact of $S(t)>0$ for all $t\in[0,t_1)$. It follows that $S(t)>0$ for all $t\geqslant 0$.

Nextly, we prove that $I(t),C(t)$ and $B(t)$ are positive for all $t\geqslant 0$. Assume the contrary and let

$$H(t)=\min\{I(t),C(t),B(t)\},\quad t\in\mathbb{R}^+.$$

It is clear that $H(0)>0$. Assuming that there exists a $t_2>0$ such that $H(t_2)=0$ and $H(t)>0$ for all $t\in[0,t_2)$.

If $H(t_2)=I(t_2)=0$, then $C(t)\geqslant 0,B(t)\geqslant 0$ for all $t\in[0,t_2]$. Solving $I(t)$ in the Eq. (2.3b), we obtain

$$\begin{aligned}I(t_2)=e^{-(\mu+\nu+\delta)t_2}\Bigg[I(0)+\int_0^{t_2}pe^{-\mu\tau}S(\theta-\tau)\Bigg(&\beta_I I(\theta-\tau)+\beta_C C(\theta-\tau)\\&+\frac{\beta_B B(\theta-\tau)}{K+B(\theta-\tau)}\Bigg)e^{(\mu+\nu+\delta)\theta}\mathrm{d}\theta\Bigg]\\ \geqslant e^{-(\mu+\nu+\delta)t_2}I(0)>0,&\end{aligned}$$

which leads to a contradiction. Therefore, we obtain $I(t)>0$ for all $t\geqslant 0$. In a similar way, it can also be shown that $C(t),B(t)>0$ for all $t\geqslant 0$. This completes the proof. □

Theorem 3.2. *Any positive solution of system* (2.3) *is ultimately bounded, and the following set:*

$$\Omega=\left\{\big(S(t),I(t),C(t),B(t)\big)\in\mathbb{R}^4_+ : S(t)+e^{\mu\tau}\big(I(t+\tau)+C(t+\tau)\big)\leqslant\frac{\Lambda}{\mu},B(t)\leqslant\frac{\max\{\xi_1,\xi_2\}\Lambda}{\mu r}\right\}$$

is positively invariant for system (2.3).

Proof. Firstly, we define

$$G(t)=S(t)+e^{\mu\tau}I(t+\tau)+e^{\mu\tau}C(t+\tau).$$

Calculating the derivative of $G(t)$ in respect to t along positive solution of system (2.3), it follows that

$$\begin{aligned}\dot{G}(t)&=\Lambda-\mu\big(S(t)+e^{\mu\tau}I(t+\tau)+e^{\mu\tau}C(t+\tau)\big)-\nu\big(e^{\mu\tau}I(t+\tau)+e^{\mu\tau}C(t+\tau)\big)\\&\leqslant\Lambda-\mu G(t),\end{aligned}$$

where $G(0)=S(0)+e^{\mu\tau}I(\tau)+e^{\mu\tau}C(\tau)$, so

$$\limsup_{t\to\infty}G(t)\leqslant\frac{\Lambda}{\mu}.$$

Hence, for $\epsilon>0$ sufficiently small, there is a $T_1>0$ such that when $t>T_1$,

$$G(t)=S(t)+e^{\mu\tau}I(t+\tau)+e^{\mu\tau}C(t+\tau)<\frac{\Lambda}{\mu}+\epsilon.$$

Furthermore, from the Eq. (2.3d), for $t>T_1+\tau$,

$$\dot{B}(t)=\xi_1I(t)+\xi_2C(t)-rB(t)\leqslant\max\{\xi_1,\xi_2\}\left(\frac{\Lambda}{\mu}+\epsilon\right)-rB(t),$$

which yields

$$\limsup_{t\to\infty}B(t)\leqslant\frac{\max\{\xi_1,\xi_2\}\Lambda}{\mu r}+\frac{\max\{\xi_1,\xi_2\}\epsilon}{r}.$$

Since this inequality holds true for arbitrary $\epsilon>0$ sufficiently small, we conclude that

$$\limsup_{t\to\infty}B(t)\leqslant\frac{\max\{\xi_1,\xi_2\}\Lambda}{\mu r}.$$

Therefore, $S(t),I(t),C(t)$ and $B(t)$ are ultimately bounded. This completes the proof. □

3.2 The basic reproduction number and feasible equilibria

It is easy to calculate the disease-free equilibrium of system (2.3) $E_0=(S_0,0,0,0)$, where $S_0=\Lambda/\mu$. Nextly, we calculate the basic reproduction number of system (2.3) based on the theoretical analysis in [51, 52].

Linearizing the last three equations of system (2.3) at E_0 into the following system:

$$\begin{cases}\dot{I}(t)=pe^{-\mu\tau}S_0\left[\beta_II(t-\tau)+\beta_CC(t-\tau)+\dfrac{\beta_B}{K}B(t-\tau)\right]-(\mu+\nu+\delta)I(t),\\ \dot{C}(t)=(1-p)e^{-\mu\tau}S_0\left[\beta_II(t-\tau)+\beta_CC(t-\tau)+\dfrac{\beta_B}{K}B(t-\tau)\right]\\ \qquad\quad+\delta I(t)-(\mu+\nu)C(t),\\ \dot{B}(t)=\xi_1I(t)+\xi_2C(t)-rB(t).\end{cases}\tag{3.1}$$

We denote $\mathbb{C}_1$ the Banach space $C([-\tau,0],\mathbb{R}^3)$ of continuous functions from $[-\tau,0]$ to $\mathbb{R}^3$. This space is equipped with the supremum norm $\|\psi\| = \sup_{t\in[-\tau,0]}|\psi(t)|$ for $\psi = (\phi_2,\phi_3,\phi_4) \in \mathbb{C}_1$. Let $\mathcal{L}(\mathbb{C}_1,\mathbb{R}^3)$ be the space of bounded linear operators from $\mathbb{C}_1$ to $\mathbb{R}^3$. Clearly, system (3.1) has a form (see, for example, [51, Eq. (11.1)]), which is

$$\frac{d\psi(t)}{dt} = F\psi_t - V\psi(t), \quad t \geqslant 0,$$

where $\psi_t = \psi(t+\theta)$ for $\theta\in[-\tau,0], F\in\mathcal{L}(\mathbb{C}_1,\mathbb{R}^3), V\in\mathcal{L}(\mathbb{R}^3,\mathbb{R}^3)$, that is,

$$F\psi_t = \begin{pmatrix} pe^{-\mu\tau}S_0\left[\beta_I\phi_2(-\tau)+\beta_C\phi_3(-\tau)+\dfrac{\beta_B}{K}\phi_4(-\tau)\right] \\ (1-p)e^{-\mu\tau}S_0\left[\beta_I\phi_2(-\tau)+\beta_C\phi_3(-\tau)+\dfrac{\beta_B}{K}\phi_4(-\tau)\right] \\ 0 \end{pmatrix},$$

$$V = \begin{pmatrix} \mu+\nu+\delta & 0 & 0 \\ -\delta & \mu+\nu & 0 \\ -\xi_1 & -\xi_2 & r \end{pmatrix}.$$

For $F\in\mathcal{L}(\mathbb{C}_1,\mathbb{R}^3)$, we define $\hat{F}\in\mathcal{L}(\mathbb{R}^3,\mathbb{R}^3)$ by

$$\hat{F}\psi = F(\hat{\psi}), \quad \forall\psi\in\mathbb{R}^3,$$

where $\hat{\psi}(\theta) = \psi$ for any $\theta\in[-\tau,0]$. Clearly, $\hat{F}$ can be regarded as an 3×3 matrix. Here, it is given by

$$\hat{F} = \begin{pmatrix} \dfrac{p\Lambda\beta_I e^{-\mu\tau}}{\mu} & \dfrac{p\Lambda\beta_C e^{-\mu\tau}}{\mu} & \dfrac{p\Lambda\beta_B e^{-\mu\tau}}{K\mu} \\ \dfrac{(1-p)\Lambda\beta_I e^{-\mu\tau}}{\mu} & \dfrac{(1-p)\Lambda\beta_C e^{-\mu\tau}}{\mu} & \dfrac{(1-p)\Lambda\beta_B e^{-\mu\tau}}{K\mu} \\ 0 & 0 & 0 \end{pmatrix}.$$

By [51, Corollary 11.1.1] and a direct calculation, we obtain

$$\begin{aligned} \mathcal{R}_0 &= \rho(\hat{F}V^{-1}) = \mathcal{R}_{0SI}+\mathcal{R}_{0SC}+\mathcal{R}_{0SIB}+\mathcal{R}_{0SCB} \\ &= \frac{p\Lambda e^{-\mu\tau}\beta_I}{\mu(\mu+\nu+\delta)} + \frac{[(1-p)(\mu+\nu)+\delta]\Lambda e^{-\mu\tau}\beta_C}{\mu(\mu+\nu)(\mu+\nu+\delta)} \\ &\quad + \frac{p\xi_1\Lambda e^{-\mu\tau}\beta_B}{Kr\mu(\mu+\nu+\delta)} + \frac{[(1-p)(\mu+\nu)+\delta]\xi_2\Lambda e^{-\mu\tau}\beta_B}{Kr\mu(\mu+\nu)(\mu+\nu+\delta)}, \end{aligned}$$

where $\rho(\hat{F}V^{-1})$ denotes the spectral radius of the matrix $\hat{F}V^{-1}$. Moreover, each of these quantities has its own biological significance. $\mathcal{R}_{0SI}$ ($\mathcal{R}_{0SC}$) is the average number of the infected sheep by a single acutely (chronically) infected sheep in a fully susceptible sheep.

$\mathcal{R}_{0SIB}$ ($\mathcal{R}_{0SCB}$) is the average number of the infected sheep by the brucella which are excreted into the environment by the acutely (chronically) infected sheep. Therefore, $\mathcal{R}_0$ denotes the total average number of infections.

It is easy to see that if $\mathcal{R}_0 > 1$, in addition to the disease-free equilibrium E_0, system (2.3) has a unique endemic equilibrium $E^* = (S^*, I^*, C^*, B^*)$, where

$$\begin{aligned} S^* &= \frac{\Lambda(K+B^*)}{(K+B^*)[\mu+\beta_I I^*+\beta_C C^*]+\beta_B B^*}, \\ I^* &= \frac{-a_1+\sqrt{a_1^2-4a_2a_0}}{2a_2}, \\ C^* &= \frac{[(1-p)(\mu+\nu)+\delta]I^*}{p(\mu+\nu)}, \\ B^* &= \frac{\xi_1 I^*+\xi_2 C^*}{r}, \end{aligned} \tag{3.2}$$

here

$$\begin{aligned} a_0 &= p^2(\mu+\nu)^2\mu(\mu+\nu+\delta)Kr(1-\mathcal{R}_0) < 0, \\ a_1 &= \left(1+\frac{\beta_B}{\mu}-\mathcal{R}_{0SI}-\mathcal{R}_{0SC}\right)p\mu(\mu+\nu)(\mu+\nu+\delta)[p\xi_1(\mu+\nu)+(1-p)(\mu+\nu)\xi_2+\delta\xi_2] \\ &\quad +(\mathcal{R}_{0SI}+\mathcal{R}_{0SC})\frac{p\mu Kr(\mu+\nu)^2(\mu+\nu+\delta)^2}{\Lambda e^{-\mu\tau}}, \\ a_2 &= \frac{(\mathcal{R}_{0SI}+\mathcal{R}_{0SC})\mu(\mu+\nu)(\mu+\nu+\delta)^2[p\xi_1(\mu+\nu)+(1-p)(\mu+\nu)\xi_2+\delta\xi_2]}{\Lambda e^{-\mu\tau}} > 0. \end{aligned}$$

4 Local stability

In this section, we discuss the local stability of feasible equilibrium of system (2.3) by analyzing the distribution of roots of the corresponding characteristic equations.

Theorem 4.1. *The disease-free equilibrium E_0 is locally asymptotically stable if $\mathcal{R}_0 < 1$ and unstable if $\mathcal{R}_0 > 1$.*

Proof. The characteristic equation of the system (2.3) at disease-free equilibrium E_0 is

$$\begin{aligned} (\lambda+\mu)\Big\{&[(\lambda+\mu+\nu)(1-p)+\delta][(\lambda+r)K\beta_C+\xi_2\beta_B]+p(\lambda+\mu+\nu)[(\lambda+r)K\beta_I+\xi_1\beta_B] \\ &-\frac{K\mu(\lambda+r)(\lambda+\mu+\nu)(\lambda+\mu+\nu+\delta)}{\Lambda e^{-(\lambda+\mu)\tau}}\Big\} = 0. \end{aligned} \tag{4.1}$$

Clearly, Eq. (4.1) always has a negative root $\lambda_1=-\mu<0$. The other roots of Eq. (4.1) are determined by the following equation:

$$\begin{aligned}&[(\lambda+\mu+\nu)(1-p)+\delta][(\lambda+r)K\beta_C+\xi_2\beta_B]+p(\lambda+\mu+\nu)[(\lambda+r)K\beta_I+\xi_1\beta_B]\\=&\frac{K\mu(\lambda+r)(\lambda+\mu+\nu)(\lambda+\mu+\nu+\delta)}{\Lambda e^{-(\lambda+\mu)\tau}}.\end{aligned}\tag{4.2}$$

Let $\lambda_0=\mathrm{Re}\lambda_0+i\mathrm{Im}\lambda_0$ ($\mathrm{Re}\lambda_0\geqslant 0$) be a root of Eq. (4.2). When $\mathcal{R}_0<1$, we obtain that

$$\begin{aligned}1=&\left|\left\{\frac{[(\lambda_0+\mu+\nu)(1-p)+\delta][(\lambda_0+r)K\beta_C+\xi_2\beta_B]}{(\lambda_0+r)(\lambda_0+\mu+\nu)(\lambda_0+\mu+\nu+\delta)}+\frac{p[(\lambda_0+r)K\beta_I+\xi_1\beta_B]}{(\lambda_0+r)(\lambda_0+\mu+\nu+\delta)}\right\}\frac{\Lambda e^{-(\lambda_0+\mu)\tau}}{K\mu}\right|\\
\leqslant&\left|\frac{\mu+\nu+\delta}{\lambda_0+\mu+\nu+\delta}\right|\cdot\left|\frac{p\Lambda e^{-\mu\tau}\beta_I}{\mu(\mu+\nu+\delta)}+\frac{[(\lambda_0+\mu+\nu)(1-p)+\delta]\Lambda e^{-\mu\tau}\beta_C}{\mu(\mu+\nu)(\mu+\nu+\delta)}\cdot\frac{\mu+\nu}{\lambda_0+\mu+\nu}\right.\\
&\qquad+\frac{p\xi_1\Lambda e^{-\mu\tau}\beta_B}{K\mu(\lambda_0+r)(\mu+\nu+\delta)}\\
&\qquad\left.+\frac{[(\lambda_0+\mu+\nu)(1-p)+\delta]\xi_2\Lambda e^{-\mu\tau}\beta_B}{K\mu(\mu+\nu)(\lambda_0+r)(\mu+\nu+\delta)}\cdot\frac{\mu+\nu}{\lambda_0+\mu+\nu}\right|\\
\leqslant&\mathcal{R}_{0SI}+\left(\mathcal{R}_{0SC}+\frac{r\mathcal{R}_{0SCB}}{|\lambda_0+r|}\right)\cdot\left|\frac{[(\lambda_0+\mu+\nu)(1-p)+\delta](\mu+\nu)}{[(1-p)(\mu+\nu)+\delta](\lambda_0+\mu+\nu)}\right|+\frac{r\mathcal{R}_{0SIB}}{|\lambda_0+r|}\\
\leqslant&\mathcal{R}_{0SI}+\mathcal{R}_{0SC}+\mathcal{R}_{0SCB}+\mathcal{R}_{0SIB}=\mathcal{R}_0<1,\end{aligned}$$

which leads to a contradiction, so the roots of characteristic equation (4.2) all have negative real parts. Therefore, when $\mathcal{R}_0<1$, the disease-free equilibrium E_0 is locally asymptotically stable.

When $\mathcal{R}_0>1$, let

$$F(\lambda,\tau)=1-\left\{\frac{[(\lambda+\mu+\nu)(1-p)+\delta][(\lambda+r)K\beta_C+\xi_2\beta_B]}{(\lambda+r)(\lambda+\mu+\nu)(\lambda+\mu+\nu+\delta)}+\frac{p[(\lambda+r)K\beta_I+\xi_1\beta_B]}{(\lambda+r)(\lambda+\mu+\nu+\delta)}\right\}\frac{\Lambda e^{-(\lambda+\mu)\tau}}{K\mu},$$

then $F(0,\tau)=1-\mathcal{R}_0<0$ and $\lim_{\lambda\to+\infty}F(\lambda,\tau)=1$ for $\lambda\in\mathbb{R}$. Noting that $F(\lambda,\tau)$ is a continuous function in respect to λ, so $F(\lambda,\tau)=0$ has at least one positive solution. Accordingly, Eq. (4.2) has at least one positive real root. Therefore, the disease-free equilibrium E_0 is unstable if $\mathcal{R}_0>1$. □

Theorem 4.2. *The endemic equilibrium E^* is locally asymptotically stable if $\mathcal{R}_0>1$.*

Proof. The characteristic equation of the system (2.3) at endemic equilibrium E^* is

$$\begin{aligned}&(\lambda+r)(\lambda+\mu+\nu)(\lambda+\mu+\nu+\delta)(\lambda+\mu+M_1)\\
=&(\lambda+\mu)\left\{(\lambda+r)\left\{(\lambda+\mu+\nu)p\beta_I+[(\lambda+\mu+\nu)(1-p)+\delta]\beta_C\right\}\right.\\
&\qquad\left.+\frac{\left\{(\lambda+\mu+\nu)p\xi_1+[(\lambda+\mu+\nu)(1-p)+\delta]\xi_2\right\}K\beta_B}{(K+B^*)^2}\right\}S^*e^{-(\lambda+\mu)\tau},\end{aligned}\tag{4.3}$$

where $M_1=\beta_I I^*+\beta_C C^*+\beta_B B^*/(K+B^*)$.

Let $\lambda_0 = \mathrm{Re}\lambda_0 + i\mathrm{Im}\lambda_0$ ($\mathrm{Re}\lambda_0 \geqslant 0$) be a root of Eq. (4.3). It is obvious that

$$|\lambda_0+\mu+M_1| \geqslant |(\lambda_0+\mu)e^{-\lambda_0\tau}|, \quad \left|\frac{r}{\lambda_0+r}\right| \leqslant 1, \quad \frac{K}{K+B^*} < 1,$$

and

$$\left|\frac{[(1-p)(\lambda_0+\mu+\nu)+\delta](\mu+\nu)}{[(1-p)(\mu+\nu)+\delta](\lambda_0+\mu+\nu)}\right| \leqslant 1.$$

From Eq. (3.2), it can be derived that

$$I^*+C^* = \frac{\mu+\nu+\delta}{p(\mu+\nu)}I^* = \frac{\mu+\nu+\delta}{(1-p)(\mu+\nu)+\delta}C^*.$$

Substituting E^* into system (2.3) and adding the Eqs. (2.3b) and (2.3c), we obtain

$$\begin{cases} \beta_I S^* e^{-\mu\tau} = \dfrac{(\mu+\nu)(I^*+C^*)\beta_I}{M_1}, \\ \beta_C S^* e^{-\mu\tau} = \dfrac{(\mu+\nu)(I^*+C^*)\beta_C}{M_1}, \\ \dfrac{\beta_B S^* e^{-\mu\tau}}{K+B^*} = \dfrac{(\mu+\nu)(I^*+C^*)\beta_B}{(K+B^*)M_1}. \end{cases} \tag{4.4}$$

On substituting Eq. (4.4) into Eq. (4.3), we obtain that

$$\begin{aligned} &\left|\left\{\frac{(\lambda_0+r)\{(\lambda_0+\mu+\nu)p\beta_I+[(\lambda_0+\mu+\nu)(1-p)+\delta]\beta_C\}}{(\lambda_0+r)(\lambda_0+\mu+\nu)}\right.\right. \\ &\qquad \left.\left.+\frac{\{(\lambda_0+\mu+\nu)p\xi_1+[(\lambda_0+\mu+\nu)(1-p)+\delta]\xi_2\}K\beta_B}{(\lambda_0+r)(\lambda_0+\mu+\nu)(K+B^*)^2}\right\}S^*e^{-\mu\tau}\right| \\ \leqslant &\left|\frac{(\mu+\nu+\delta)K\beta_B}{(\lambda_0+r)(K+B^*)^2M_1}\right|\left\{\xi_1 I^*+\xi_2 C^*\left|\frac{(\mu+\nu)[(1-p)(\lambda_0+\mu+\nu)+\delta]}{(\lambda_0+\mu+\nu)[(1-p)(\mu+\nu)+\delta]}\right|\right\} \\ &\quad +\frac{\mu+\nu+\delta}{M_1}\left\{\beta_I I^*+\beta_C C^*\left|\frac{(\mu+\nu)[(1-p)(\lambda_0+\mu+\nu)+\delta]}{(\lambda_0+\mu+\nu)[(1-p)(\mu+\nu)+\delta]}\right|\right\} \\ \leqslant &\frac{\mu+\nu+\delta}{M_1}\left[\beta_I I^*+\beta_C C^*+\frac{\beta_B B^* Kr}{(K+B^*)^2|\lambda_0+r|}\right] \\ < &\frac{\mu+\nu+\delta}{M_1}\left(\beta_I I^*+\beta_C C^*+\frac{\beta_B B^*}{K+B^*}\right) \\ = &\mu+\nu+\delta \leqslant |\lambda_0+\mu+\nu+\delta|. \end{aligned} \tag{4.5}$$

By comparing Eq. (4.3) with inequality (4.5), it is obvious that $\lambda_0 = \mathrm{Re}\lambda_0 + i\mathrm{Im}\lambda_0$, ($\mathrm{Re}\lambda_0 \geqslant 0$) is not a root of Eq. (4.3), which contradicts the assumption. Consequently, all roots of the characteristic equation (4.3) must have negative real parts. Therefore, when $\mathcal{R}_0 > 1$, the endemic equilibrium E^* is locally asymptotically stable. □

5 Global stability

In this section, we discuss the global stability of the disease-free equilibrium and endemic equilibrium of system (2.3) by constructing Lyapunov functionals and using LaSalle's invariance principle.

Theorem 5.1. *If $\mathcal{R}_0<1$, the disease-free equilibrium E_0 of system* (2.3) *is globally asymptotically stable in Ω.*

Proof. Let $(S(t),I(t),C(t),B(t))$ be any positive solution of system (2.3) with initial condition (2.4). Define

$$\begin{aligned} V_1(t)=S(t)-S_0-S_0\ln\frac{S(t)}{S_0}+c_1e^{\mu\tau}I(t)+c_2e^{\mu\tau}C(t)+c_3B(t),\\ +\int_{t-\tau}^{t}S(\theta)\left[\beta_II(\theta)+\beta_CC(\theta)+\frac{\beta_BB(\theta)}{K+B(\theta)}\right]\mathrm{d}\theta, \end{aligned} \tag{5.1}$$

where

$$\begin{aligned} c_1&=\frac{[(\mu+\nu)(\mu+\nu+\delta)e^{\mu\tau}(1-\mathcal{R}_{0SC})+p\delta\beta_CS_0]\xi_1+[(1-p)\beta_IS_0+\delta e^{\mu\tau}](\mu+\nu+\delta)\xi_2}{\{p(\mu+\nu)\xi_1+[(1-p)(\mu+\nu)+\delta]\xi_2\}(\mu+\nu+\delta)e^{\mu\tau}},\\ c_2&=\frac{p\beta_CS_0\xi_1+(\mu+\nu+\delta)e^{\mu\tau}(1-\mathcal{R}_{0SI})\xi_2}{\{p(\mu+\nu)\xi_1+[(1-p)(\mu+\nu)+\delta]\xi_2\}e^{\mu\tau}},\\ c_3&=\frac{(\mu+\nu)(\mu+\nu+\delta)e^{\mu\tau}(1-\mathcal{R}_{0SI}-\mathcal{R}_{0SC})}{p(\mu+\nu)\xi_1+[(1-p)(\mu+\nu)+\delta]\xi_2}. \end{aligned} \tag{5.2}$$

Calculating the derivative of $V_1(t)$ along positive solutions of system (2.3) yields

$$\begin{aligned} \dot{V}_1(t)=&\left(1-\frac{S_0}{S(t)}\right)\left[\Lambda-\mu S(t)-\beta_IS(t)I(t)-\beta_CS(t)C(t)-\frac{\beta_BS(t)B(t)}{K+B(t)}\right]\\ &+[c_1p+c_2(1-p)]S(t-\tau)\left[\beta_II(t-\tau)+\beta_CC(t-\tau)+\frac{\beta_BB(t-\tau)}{K+B(t-\tau)}\right]\\ &+c_3[\xi_1I(t)+\xi_2C(t)-rB(t)]+\beta_IS(t)I(t)+\beta_CS(t)C(t)+\frac{\beta_BS(t)B(t)}{K+B(t)}\\ &-\beta_IS(t-\tau)I(t-\tau)-\beta_CS(t-\tau)C(t-\tau)-\frac{\beta_BS(t-\tau)B(t-\tau)}{K+B(t-\tau)}\\ &-c_1e^{\mu\tau}(\mu+\nu+\delta)I(t)+c_2e^{\mu\tau}\delta I(t)-c_2e^{\mu\tau}(\mu+\nu)C(t). \end{aligned} \tag{5.3}$$

On substituting $\Lambda=\mu S_0$ into (5.3), we obtain that

$$\dot{V}_1(t)=-\frac{\mu\big(S(t)-S_0\big)^2}{S(t)}+\frac{\beta_BS_0B(t)}{K+B(t)}+\big[\beta_IS_0+c_3\xi_1+c_2e^{\mu\tau}\delta-c_1e^{\mu\tau}(\mu+\nu+\delta)\big]I(t)$$

$$+[c_1p+c_2(1-p)]S(t-\tau)\left[\beta_I I(t-\tau)+\beta_C C(t-\tau)+\frac{\beta_B B(t-\tau)}{K+B(t-\tau)}\right]$$
$$-\beta_I S(t-\tau)I(t-\tau)-\beta_C S(t-\tau)C(t-\tau)-\frac{\beta_B S(t-\tau)B(t-\tau)}{K+B(t-\tau)}$$
$$+\left[\beta_C S_0+c_3\xi_2-c_2e^{\mu\tau}(\mu+\nu)\right]C(t)-c_3rB(t). \tag{5.4}$$

On substituting (5.2) into (5.4), we obtain that

$$\dot{V}_1=-\frac{\mu\big(S(t)-S_0\big)^2}{S(t)}-\frac{Kre^{\mu\tau}(\mu+\nu)(\mu+\nu+\delta)(1-\mathcal{R}_0)B(t)}{\big(K+B(t)\big)\{p(\mu+\nu)\xi_1+[(1-p)(\mu+\nu)+\delta]\xi_2\}}$$
$$-\frac{re^{\mu\tau}(\mu+\nu)(\mu+\nu+\delta)(1-\mathcal{R}_{0SI}-\mathcal{R}_{0SC})B^2(t)}{\big(K+B(t)\big)\{p(\mu+\nu)\xi_1+[(1-p)(\mu+\nu)+\delta]\xi_2\}}. \tag{5.5}$$

When $\mathcal{R}_0<1$, it follows from (5.5) that $\dot{V}_1(t)\leqslant 0$ and $\dot{V}_1(t)=0$ if and only if

$$\big(S(t),I(t),C(t),B(t)\big)=(S_0,0,0,0).$$

Clearly, $\{E_0\}$ is the largest invariant subset of $\{(S(t),I(t),C(t),B(t)):\dot{V}_1(t)=0\}$. Therefore, by Theorem 4.1 and LaSalle's invariance principle [15], the equilibrium E_0 is globally asymptotically stable. This completes the proof. □

Theorem 5.2. *If $\mathcal{R}_0>1$, the endemic equilibrium E^* of system* (2.3) *is globally asymptotically stable in Ω.*

Proof. Let $(S(t),I(t),C(t),B(t))$ be any positive solution of system (2.3) with initial condition (2.4) and

$$M=\beta_I S^*I^*+\beta_C S^*C^*+\frac{\beta_B S^*B^*}{K+B^*}.$$

Define

$$V_2(t)=S^*G\left(\frac{S(t)}{S^*}\right)+d_1e^{\mu\tau}I^*G\left(\frac{I(t)}{I^*}\right)+d_2e^{\mu\tau}C^*G\left(\frac{C(t)}{C^*}\right)+d_3B^*G\left(\frac{B(t)}{B^*}\right) \tag{5.6}$$
$$+\int_{t-\tau}^{t}\left[A_1G\left(\frac{S(\theta)I(\theta)}{S^*I^*}\right)+A_2G\left(\frac{S(\theta)C(\theta)}{S^*C^*}\right)+A_3G\left(\frac{S(\theta)B(\theta)(K+B^*)}{S^*B^*(K+B(\theta))}\right)\right]\mathrm{d}\theta,$$

where

$$A_1=\beta_I S^*I^*,\quad A_2=\beta_C S^*C^*,\quad A_3=\frac{\beta_B S^*B^*}{K+B^*},$$

and

$$d_1=\frac{(1-p)(A_1+d_3\xi_1I^*)+\delta e^{\mu\tau}I^*}{p[(1-p)M+\delta e^{\mu\tau}I^*]}, \tag{5.7a}$$

$$d_2=\frac{A_2+d_3\xi_2C^*}{(1-p)M+\delta e^{\mu\tau}I^*}, \tag{5.7b}$$

$$d_3 = \frac{A_3}{\xi_1 I^* + \xi_2 C^*}. \tag{5.7c}$$

Since the function $G(x) = x - 1 - \ln x \geqslant 0$ for all $x > 0$ and $G(x) = 0$ holds if and only if $x = 1$. Hence, $V_2(t)$ is positively definite.

Calculating the derivative of $V_2(t)$ along positive solutions of system (2.3) yields

$$\begin{aligned}
\dot{V}_2(t) = {} & \left(1 - \frac{S^*}{S(t)}\right)\left(\Lambda - \mu S(t) - \beta_I S(t) I(t) - \beta_C S(t) C(t) - \frac{\beta_B S(t) B(t)}{K + B(t)}\right) \\
& + d_1 e^{\mu\tau}\left(1 - \frac{I^*}{I(t)}\right)\left\{ p e^{-\mu\tau} S(t-\tau)\left[\beta_I I(t-\tau) + \beta_C C(t-\tau) + \frac{\beta_B B(t-\tau)}{K + B(t-\tau)}\right]\right. \\
& \qquad \left. - (\mu + \nu + \delta) I(t)\right\} \\
& + A_1\left[\frac{S(t) I(t)}{S^* I^*} - \frac{S(t-\tau) I(t-\tau)}{S^* I^*} + \ln\frac{S(t-\tau) I(t-\tau)}{S(t) I(t)}\right] \\
& + d_2 e^{\mu\tau}\left(1 - \frac{C^*}{C(t)}\right)\left\{\delta I(t) - (\mu + \nu) C(t) + (1-p) e^{-\mu\tau} S(t-\tau)\right. \\
& \qquad \left. \times \left[\beta_I I(t-\tau) + \beta_C C(t-\tau) + \frac{\beta_B B(t-\tau)}{K + B(t-\tau)}\right]\right\} \\
& + d_3\left(1 - \frac{B^*}{B(t)}\right)\left(\xi_1 I(t) + \xi_2 C(t) - r B(t)\right) \\
& + A_2\left[\frac{S(t) C(t)}{S^* C^*} - \frac{S(t-\tau) C(t-\tau)}{S^* C^*} + \ln\frac{S(t-\tau) C(t-\tau)}{S(t) C(t)}\right] \\
& + A_3\left[\frac{S(t) B(t)(K + B^*)}{S^* B^*\big(K + B(t)\big)} - \frac{S(t-\tau) B(t-\tau)(K + B^*)}{S^* B^*\big(K + B(t-\tau)\big)}\right. \\
& \qquad \left. + \ln\frac{S(t-\tau) B(t-\tau)\big(K + B(t)\big)}{S(t) B(t)\big(K + B(t-\tau)\big)}\right].
\end{aligned} \tag{5.8}$$

On substituting

$$\Lambda = \mu S^* + \beta_I S^* I^* + \beta_C S^* C^* + \frac{\beta_B S^* B^*}{K + B^*}$$

into (5.8), we obtain

$$\begin{aligned}
\dot{V}_2(t) = {} & -\frac{\mu\big(S(t) - S^*\big)^2}{S(t)} + (A_1 + A_2 + A_3)\left(2 - \frac{S^*}{S(t)}\right) + A_1 \ln\frac{S(t-\tau) I(t-\tau)}{S(t) I(t)} \\
& + A_2 \ln\frac{S(t-\tau) C(t-\tau)}{S(t) C(t)} + A_3\left[\ln\frac{S(t-\tau) B(t-\tau)\big(K + B(t)\big)}{S(t) B(t)\big(K + B(t-\tau)\big)} + \frac{B(t)(K + B^*)}{B^*\big(K + B(t)\big)}\right] \\
& - d_1 p\left[\frac{A_1 S(t-\tau) I(t-\tau)}{S^* I(t)} + \frac{A_2 S(t-\tau) C(t-\tau) I^*}{S^* C^* I(t)} + \frac{A_3 S(t-\tau) B(t-\tau) I^* (K + B^*)}{S^* B^* I(t)\big(K + B(t-\tau)\big)}\right]
\end{aligned}$$

$$+d_3\left(\xi_1 I^*-\xi_1\frac{B^*I(t)}{B(t)}-\xi_1\frac{B(t)I^*}{B^*}+\xi_2 C^*-\xi_2\frac{B^*C(t)}{B(t)}-\xi_2\frac{B(t)C^*}{B^*}\right)$$
$$-d_2(1-p)\left[\frac{A_3S(t-\tau)B(t-\tau)C^*(K+B^*)}{S^*B^*C(t)\big(K+B(t-\tau)\big)}+\frac{A_2S(t-\tau)C(t-\tau)}{S^*C(t)}\right.$$
$$\left.+\frac{A_1S(t-\tau)I(t-\tau)C^*}{S^*I^*C(t)}+\frac{\delta e^{\mu\tau}I^*}{1-p}\frac{C^*I(t)}{C(t)I^*}-\frac{\delta e^{\mu\tau}I^*}{1-p}\right]. \tag{5.9}$$

Let $L=(1-p)M+\delta e^{\mu\tau}I^*$. On substituting (5.7) into (5.9), we obtain

$$\begin{aligned}\dot{V}_2(t)=-\frac{1}{L}\Bigg\{&[(1-p)(A_1+A_2+A_3)+\delta e^{\mu\tau}I^*]\frac{\mu(S(t)-S^*)^2}{S(t)}\\
&+(A_1+A_2+A_3)[(1-p)M+\delta e^{\mu\tau}I^*]G\left(\frac{S^*}{S(t)}\right)+\delta e^{\mu\tau}I^*A_2G\left(\frac{C^*I(t)}{C(t)I^*}\right)\\
&+\left[(1-p)\left(A_1+\frac{A_3\xi_1I^*}{\xi_1I^*+\xi_2C^*}\right)+\delta e^{\mu\tau}I^*\right]\\
&\times\left[A_2G\left(\frac{S(t-\tau)C(t-\tau)I^*}{S^*C^*I(t)}\right)\right.\\
&\left.+A_3G\left(\frac{S(t-\tau)B(t-\tau)I^*(K+B^*)}{S^*B^*I(t)\big(K+B(t-\tau)\big)}\right)+A_1G\left(\frac{S(t-\tau)I(t-\tau)}{S^*I(t)}\right)\right]\\
&+(1-p)\left(A_2+\frac{A_3\xi_2C^*}{\xi_1I^*+\xi_2C^*}\right)\\
&\times\left[A_3G\left(\frac{S(t-\tau)B(t-\tau)C^*(K+B^*)}{S^*B^*C(t)\big(K+B(t-\tau)\big)}\right)\right.\\
&\left.+A_2G\left(\frac{S(t-\tau)C(t-\tau)}{S^*C(t)}\right)+A_1G\left(\frac{S(t-\tau)I(t-\tau)C^*}{S^*I^*C(t)}\right)\right]\\
&+A_3[(1-p)M+\delta e^{\mu\tau}I^*]\\
&\times\left[G\left(\frac{K+B(t)}{K+B^*}\right)+\frac{\xi_1I^*}{\xi_1I^*+\xi_2C^*}G\left(\frac{B^*I(t)}{B(t)I^*}\right)\right.\\
&\left.+\frac{\xi_2C^*}{\xi_1I^*+\xi_2C^*}G\left(\frac{B^*C(t)}{B(t)C^*}\right)+\frac{K(B(t)-B^*)^2}{B^*(K+B^*)\big(K+B(t)\big)}\right]\Bigg\}.\end{aligned} \tag{5.10}$$

It follows from (5.10) that $\dot{V}_2(t)\leqslant 0$ and $\dot{V}_2(t)=0$ if and only if $S(t)=S^*, I(t)=I^*, C(t)=C^*$ and $B(t)=B^*$. Clearly, $\{E^*\}$ is the largest invariant subset of $\{(S(t),I(t),C(t),B(t)) : \dot{V}_2(t)=0\}$. Therefore, by Theorem 4.2 and LaSalle's invariance principle [15], the equilibrium E^* is globally asymptotically stable when $\mathcal{R}_0>1$. This completes the proof. □

6 Data fitting

Data show that in 2016, the seropositivity rate of brucellosis in livestock in Inner Mongolia was 0.42% [14]. However, since 2017, the epidemic has rebounded due to decreased local government attention, insufficient funding, challenges in regulating livestock transportation, and inadequate public health interventions. By 2020, the individual seropositivity rate in livestock stabilized, but the herd seropositivity rate remained high, with the control situation remaining complex and severe.

The data in this study are derived from the veterinary bulletins of the Ministry of Agriculture and Rural Affairs of China [28]. From it, we extract the monthly number of new cases of sheep brucellosis in Inner Mongolia from January 2016 to December 2020, which include new cases of mixed infections in sheep and cattle. Based on the ratio of cattle to sheep at the end of each year from 2016 to 2020, we adjust the data to obtain the specific monthly number of new sheep cases. On this basis, we first sum up the monthly new cases within each year to get the annual new cases, and then calculate the cumulative number of sheep brucellosis cases in Inner Mongolia from 2016 to 2020. In this section, we conduct a fitting analysis on the cumulative number of sheep brucellosis cases in Inner Mongolia from 2016 to 2020, using the year as the time unit.

Assume that $H(t)$ is the fitting cumulative number of sheep brucellosis cases at time t, and its change with time is determined by the following delay differential equation:

$$\frac{\partial H(t)}{\partial t} = e^{-\mu\tau} S(t-\tau)\left[\beta_I I(t-\tau) + \beta_C C(t-\tau) + \frac{\beta_B B(t-\tau)}{K+B(t-\tau)}\right].$$

Based on the exponential growth characteristics of sheep brucellosis cases in Inner Mongolia from 2016 to 2020, we assume that in the early stages of brucellosis transmission, E, I and C follow exponential growth curves. Then, we assume initial functions of E, I and C as follows:

$$E(t) = e^{n_0(t+\tau)}, \quad I(t) = e^{n_1(t+\tau)}, \quad C(t) = e^{n_2(t+\tau)}, \quad t \in [-\tau, 0],$$

where, n_0, n_1 and n_2 are the parameters to be estimated. Based on the cumulative number of brucellosis cases in sheep in Inner Mongolia in 2016, we further assume that

$$H(t) = e^{n_3(t+\tau)}, \quad t \in [-\tau, 0],$$

where $n_3 = 213.7122196$. Without considering the decay of Brucella in the environment,

$$B(t) = \int_{-\tau}^{t} [\xi_1 I(s) + \xi_2 C(s)] \mathrm{d}s, \quad t \in [-\tau, 0].$$

Similar to the method in [35], we denote the vector of parameters to be estimated as

$$\Theta = (\beta_I, \beta_C, \beta_B, \delta, p, K, \xi_2, n_0, n_1, n_2),$$

and the vector of the cumulative number of reported cases as

$$Y=(Y_0,Y_1,Y_2,Y_3,Y_4),$$

where Y_t represents the cumulative number of cases in the t-th year.

To reflect the statistical characteristics of the cumulative case numbers, the likelihood function is defined as follows:

$$L(Y;\Theta)=\sum_{t=0}^{4}[Y_t\cdot\ln H(t)-H(t)-\ln\Gamma(Y_t+1)],$$

where $\Gamma(x)$ is the Gamma function. Based on the likelihood function $L(Y;\Theta)$, we use the Markov Chain Monte Carlo (MCMC) algorithm to fit $H(t)$ to the cumulative case numbers with the Metropolis-Hastings (MH) algorithm employed to conduct the MCMC sampling. The sampling process include a total of 40,000 iterations, with the first 5,000 discarded as the burn-in period. We then calculate the mean values of the estimated parameters and the basic reproduction number $\mathcal{R}_0$ from the remaining 35,000 iterations. Assuming that the estimated parameters, $H(t)$, and $\mathcal{R}_0$ obey the normal distribution, we obtain the corresponding 95% confidence intervals.

The fitting results (see Fig. 2) show a good match between the fitted curve and the reported cumulative cases, indicating that the model can reasonably describe the data dynamics. Table 2 lists the means and 95% confidence intervals of the model parameters and the basic reproduction number. According to the values of $\mathcal{R}_{0SI}$ and $\mathcal{R}_{0SC}$, acutely infected sheep bring higher transmission risks for sheep brucellosis, while chronically infected sheep bring relatively lower risks. Therefore, it is essential to control the proportion of acutely infected sheep among the infected sheep and the transmission rate of acutely infected sheep.

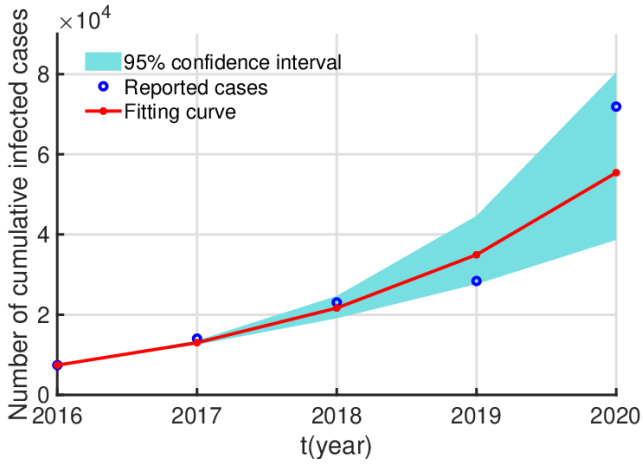

Figure 2: The fitting result of cumulative cases of sheep brucellosis.

Table 2: Values of model parameters and basic reproduction number.

Parameters	Values (year^{-1})	95% CI	Sources
Λ	24420000	None	[19]
τ	0.0417	None	[22]
μ	0.4	None	[23]
ν	0.25	None	[54]
r	4	None	[17]
ξ_1	15	None	[17]
K	54440	[53570,55528]	Fitting
ξ_2	10.062	[10.006,10.132]	Fitting
p	0.7109	[0.6073,0.7951]	Fitting
n_0	53.711	[53.582,53.795]	Fitting
n_1	183.03	[182.98,183.06]	Fitting
n_2	50.937	[50.865,50.998]	Fitting
δ	0.5033	[0.4495,0.5677]	Fitting
β_I	3.3632×10^{-8}	$[3.3365\times10^{-8},3.5253\times10^{-8}]$	Fitting
β_C	3.0232×10^{-9}	$[2.9722\times10^{-9},3.0770\times10^{-9}]$	Fitting
β_B	6.9561×10^{-11}	$[6.8769\times10^{-11},7.0321\times10^{-11}]$	Fitting
$\mathcal{R}_{0SCB}$	1.6607×10^{-7}	$[1.6585\times10^{-8},1.6748\times10^{-7}]$	Fitting
$\mathcal{R}_{0SIB}$	1.6771×10^{-7}	$[1.6063\times10^{-7},1.7158\times10^{-7}]$	Fitting
$\mathcal{R}_{0SC}$	0.1583	[0.1512,0.1613]	Fitting
$\mathcal{R}_{0SI}$	1.3857	[1.3821,1.3945]	Fitting
$\mathcal{R}_0$	1.5440	[1.5434,1.5456]	Fitting

7 Parameter sensitivity analysis

7.1 Global sensitivity analysis

In this section, we conduct sensitivity analyses of $\mathcal{R}_0, I^*, C^*$ and I^*+C^* separately using Latin hypercube sampling (LHS) and partial rank correlation coefficient (PRCC) analysis [26], and obtain the impacts of different parameters on $\mathcal{R}_0, I^*, C^*$ and I^*+C^* (see Fig. 3).

From Figs. 3(a), 3(b), and 3(d), parameters $\beta_I, \beta_C, \beta_B, p, \xi_1$ and ξ_2 exhibit positive correlations with $\mathcal{R}_0, I^*$ and I^*+C^*, whereas parameters δ,ν,r and K display negative correlations. In Fig. 3(c), parameter p is negatively correlated with C^*, while parameter δ is positively correlated with C^*, with the other parameters maintaining their respective relationships with $\mathcal{R}_0, I^*$and I^*+C^*. These findings indicate that parameters β_I, p, δ and ν have significant correlations with $\mathcal{R}_0, I^*, C^*$ and I^*+C^*. Consequently, reducing the values of parameters β_I and p, while increasing those of parameters δ and ν, can effectively control disease transmission. However, it is important to note that increasing δ or decreasing p may lead to a higher C^*.

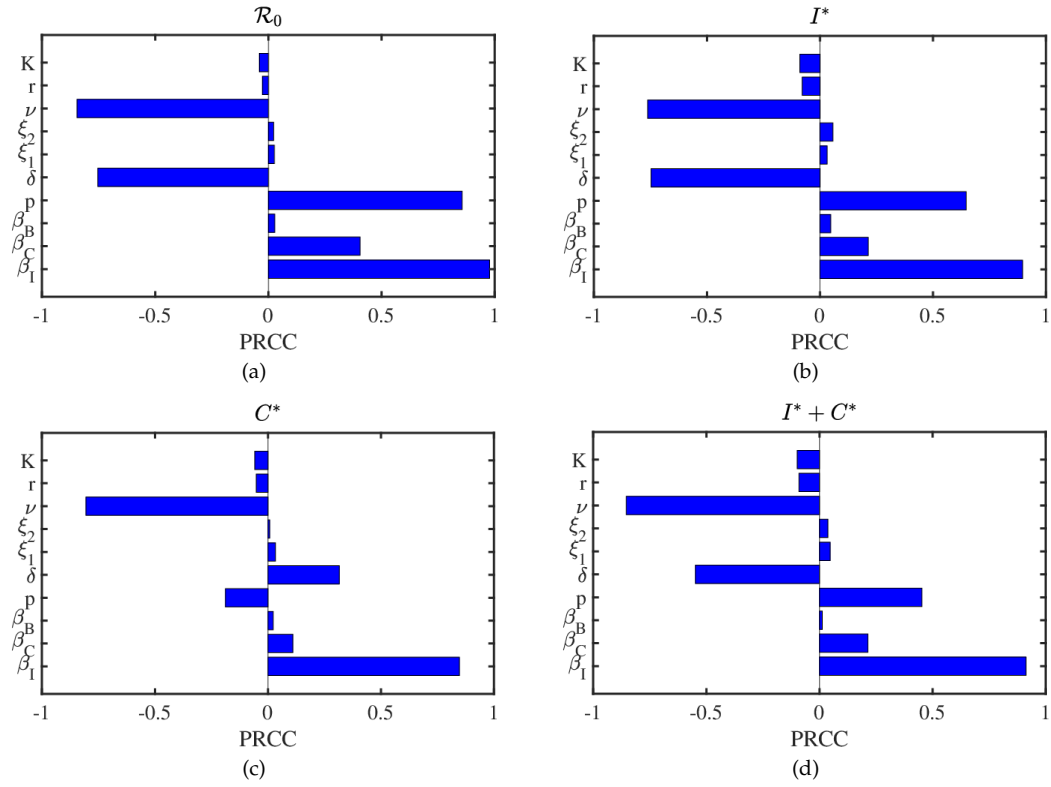

Figure 3: Partial rank correlation coefficient of parameters with respect to $\mathcal{R}_0, I^*, C^*$ and I^*+C^*.

7.2 Local sensitivity analysis

Based on the preceding partial rank correlation coefficient (PRCC) analysis, parameters β_I, p, δ and ν are recognized as critical factors in the control of disease spread. To further explore the impact of these parameters on $\mathcal{R}_0, I^*+C^*$ and C^*, we conduct local sensitivity analysis on the four parameters.

First, we conduct a sensitivity analysis on each single parameter using $\mathcal{R}_0$ and $\mathcal{R}_{0SC}$ as indicators, with the results presented in Figs. 4 and 5. Fig. 4 indicates that through early intervention, antibiotic treatment, vaccination, and culling of infected sheep, the proportion of acutely infected sheep among total infected sheep p can be reduced to less than 0.4523, the culling rate of infected sheep ν can be increased to more than 0.6699, or the transmission rate of acutely infected sheep β_I can be reduced to less than 2.025×10^{-8}. These measures can effectively control disease spread by ensuring $\mathcal{R}_0<1$. However, $\mathcal{R}_0<1$ can only be achieved if the transition rate from acute to chronic infected sheep δ exceeds 1.1625. Since $\mathcal{R}_{0SC}$ does not depend on β_I, Fig. 5 only examines the impact of p, δ and ν on $\mathcal{R}_{0SC}$. The results show that $\mathcal{R}_{0SC}$ decreases from 0.2478 to 0.1533 as p increases from 0.2 to 0.8, increases from 0.0807 to 0.1960 as δ rises from 0 to 0.9, and decreases from 0.2344 to 0.0755 as ν increases from 0.1 to 0.8.

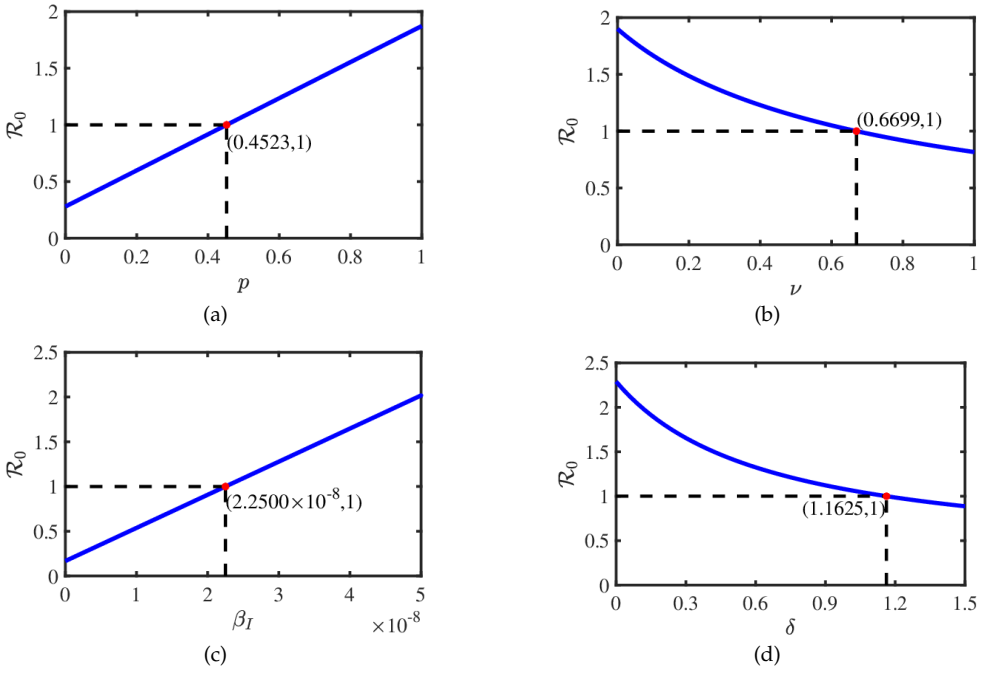

Figure 4: (a) The variation of $\mathcal{R}_0$ in term of parameter p. (b) The variation of $\mathcal{R}_0$ in term of parameter ν. (c) The variation of $\mathcal{R}_0$ in term of parameter β_I. (d) The variation of $\mathcal{R}_0$ in term of parameter δ.

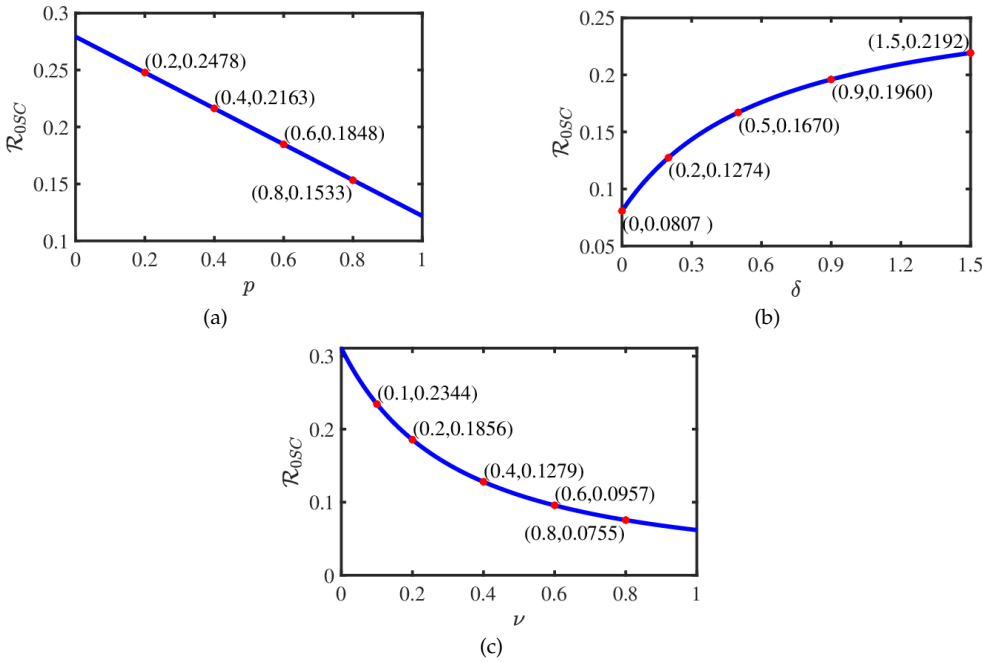

Figure 5: (a) The variation of $\mathcal{R}_{0SC}$ in term of parameter p. (b) The variation of $\mathcal{R}_{0SC}$ in term of parameter δ. (c) The variation of $\mathcal{R}_{0SC}$ in term of parameter ν.

Fig. 6 presents the contour plots of $\mathcal{R}_0$ and $\mathcal{R}_{0SC}$ for pairwise combinations of β_I, p, δ, and ν, as well as the contour plots of $\mathcal{R}_{0SC}$ for pairwise combinations of p, δ, and ν. These contours clearly delineate the threshold ranges of each parameter required to achieve $\mathcal{R}_0 < 1$ or $\mathcal{R}_{0SC} < 1$. Figs. 7(a)–7(f) illustrate the curves of $I^* + C^*$ for pairwise combinations of β_1, p, δ, and ν. From Figs. 6(a) and 7(a), it is easy to know that when ν is equal to $0, 0.2, 0.4, 0.6, 0.8$ and 1, β_I must be reduced below $1.412\times10^{-8}, 2.105\times10^{-8}, 2.713\times10^{-8}$, $3.2\times10^{-8}, 3.721\times10^{-8}$ and 4.207×10^{-8}, respectively, in order to make $I^* + C^* = 0$ and $\mathcal{R}_0 < 1$. Through comparative analysis of the other subplots in Figs. 6 and 7(a)–7(f), sim-

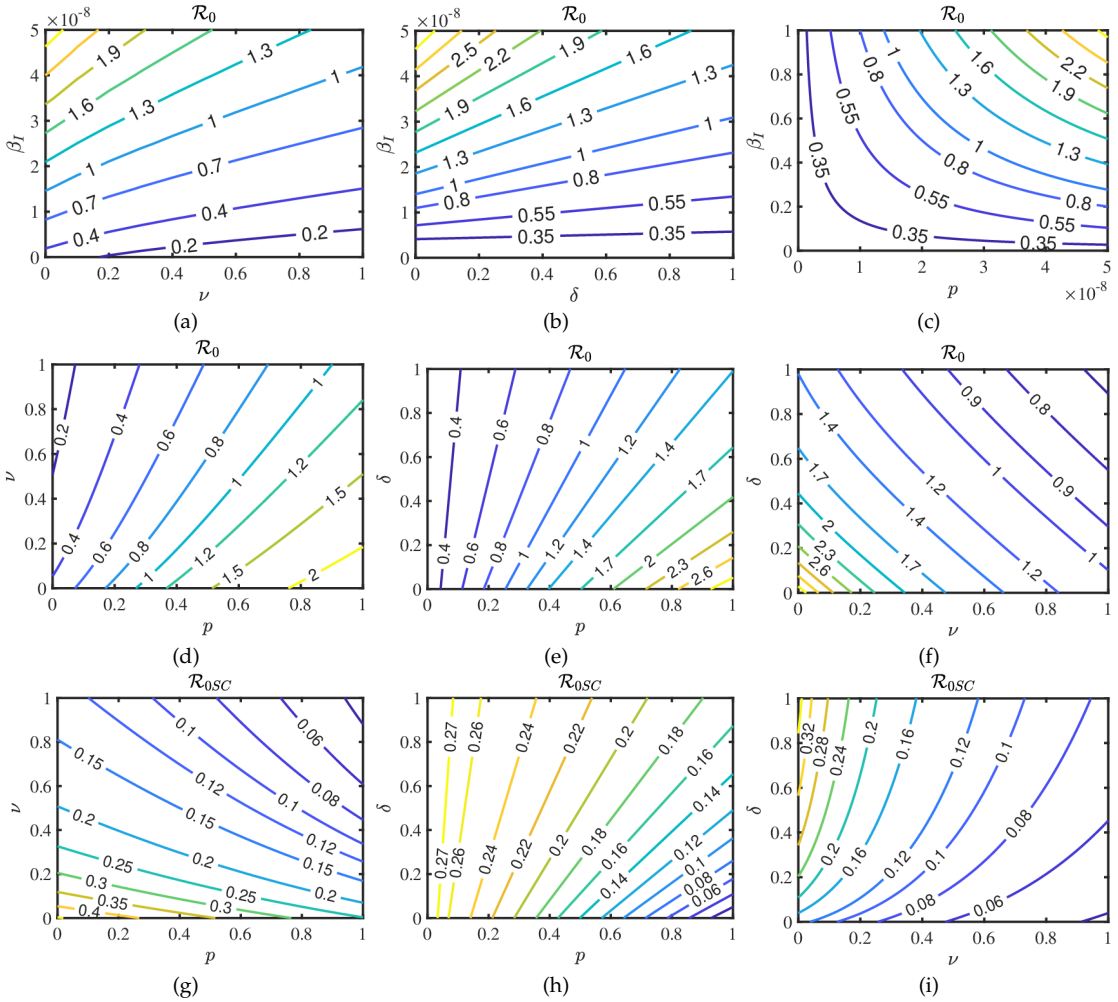

Figure 6: (a) The variation of $\mathcal{R}_0$ in term of parameters β_I and ν. (b) The variation of $\mathcal{R}_0$ in term of parameter β_I and δ. (c) The variation of $\mathcal{R}_0$ in term of parameters β_I and p. (d) The variation of $\mathcal{R}_0$ in term of parameters ν and p. (e) The variation of $\mathcal{R}_0$ in term of parameters δ and p. (f) The variation of $\mathcal{R}_0$ in term of parameters ν and δ. (g) The variation of $\mathcal{R}_{0SC}$ in term of parameters ν and p. (h) The variation of $\mathcal{R}_{0SC}$ in term of parameters p and δ. (i) The variation of $\mathcal{R}_{0SC}$ in term of parameters δ and ν.

ilar conclusions can be drawn, which can effectively control the spread of the disease. Figs. 7(g)–7(i) illustrates the curves of $\mathcal{R}_{0SC}$ for pairwise combinations of p,δ, and ν. The results show that as the parameters p and δ increase, the number of chronically infected sheep C^* first increases and then decreases. Additionally, the peak value of C^* varies with changes in p,δ, and ν. Specifically, as shown in Fig. 7(h), when $\delta=0, C^*$ can be reduced to zero by either keeping $p<0.24$ or setting $p=1$. However, a comparison with Fig. 7(e) reveals that the number of acutely infected sheep I^* significantly increases when $p=1$, which can still lead to disease outbreaks. Therefore, in disease control strategies, it is es-

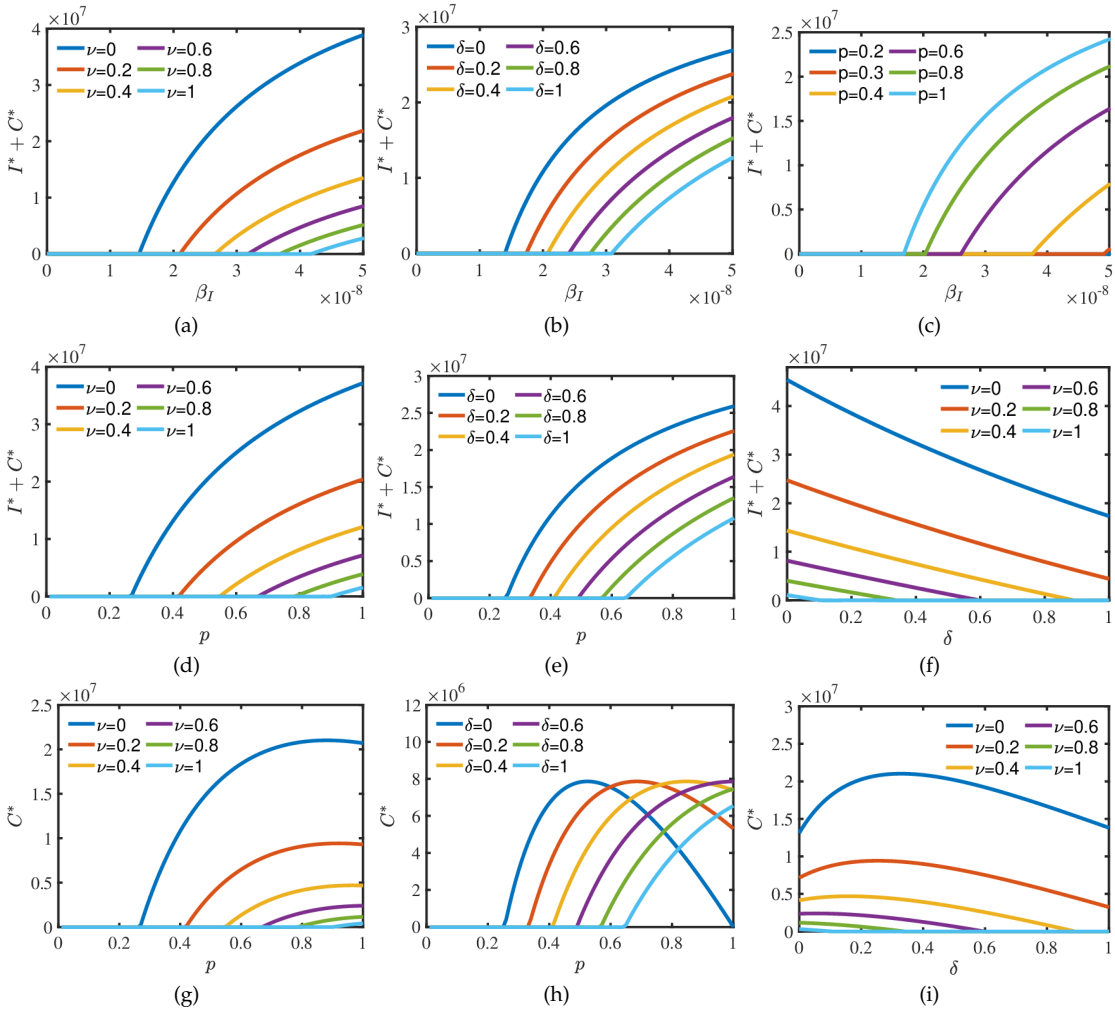

Figure 7: (a) The variation of I^*+C^* in term of parameters β_I and ν. (b) The variation of I^*+C^* in term of parameter β_I and δ. (c) The variation of I^*+C^* in term of parameters β_I and p. (d) The variation of I^*+C^* in term of parameters ν and p. (e) The variation of I^*+C^* in term of parameters δ and p. (f) The variation of I^*+C^* in term of parameters ν and δ. (g) The variation of C^* in term of parameters ν and p. (h) The variation of C^* in term of parameters p and δ. (i) The variation of C^* in term of parameters δ and ν.

sential to consider both acute and chronic infections simultaneously to comprehensively assess epidemic dynamics and formulate effective intervention measures.

Subsequently, since 2020, we implement several single control strategies:

(1) reducing the transmission rate of acute infected sheep (β_I) by rational construction of sheepfolds and avoiding contact between different herds or the transfer of sheep from foreign pastures;
(2) decreasing the proportion of acutely infected sheep (p) by conducting regular health screenings and isolating infected sheep promptly;
(3) increasing the rate of transition from acute to chronic infected sheep (δ) by providing targeted medical treatments;
(4) enhancing the culling rate due to disease (ν) by strictly enforcing health regulations.

The purpose of these strategies is to monitor the dynamic changes in the number of infected sheep over time, including $I(t)+C(t), I(t)$ and $C(t)$. To ensure that $\mathcal{R}_0<1$, based on Figs. 4(a)–4(c), we select the following parameter values: $\beta_I = 0.4\times10^{-8}, 0.8\times10^{-8}$, $1.2\times10^{-8}, 1.6\times10^{-8}, 2\times10^{-8}$; p=0,0.1,0.2,0.3,0.4, and ν=0.67,0.75,0.83,0.91,1. Using these values, we obtain the curves showing the changes in $I(t)+C(t), I(t)$, and $C(t)$ over time t (see Fig. 8). However, as shown in Fig. 4(d), $\mathcal{R}_0$ remains above 1 across the range $\delta\in[0,1]$, suggesting that adjusting δ alone is insufficient for disease control. Consequently, the effects of strategy targeting solely δ are excluded in Fig. 8.

From Figs. 8(a)-8(c), when $\beta_I = 0.4\times10^{-8}$, both $I(t)+C(t), I(t)$, and $C(t)$ continue to decline after the year 2020. As β_I increases from 0.8×10^{-8} to 1.6×10^{-8}, $I(t)+C(t)$ and $I(t)$ still show a continuous decrease after 2020. However, $C(t)$ initially increases and then decreases, with its peak value rising from 10,466 to 14,798, and the peak time shifting from January 2020 to June 2020. When $\beta_I = 2\times10^{-8}, I(t)$ continues to trend downward after 2020, but $I(t)+C(t)$ and $C(t)$ initially rise and then fall, reaching peak values of 20,736 and 11,728, respectively, with their peak times occurring in June 2020 and June 2021. From Figs. 8(d)-8(f), as the value of p increases from 0 to 0.4, $I(t)+C(t)$ and $C(t)$ initially rise and then fall after 2020, while $I(t)$ continues to decline. Specifically, the peak value of $I(t)+C(t)$ increases from 22,457 to 26,942, with the peak time postponed from June 2020 to March 2022. The peak value of $C(t)$ increases from 18,246 to 20,364, with the peak time postponed from December 2020 to August 2022. In Figs. 8(g)-8(i), only when ν=0.67, $I(t)+C(t), I(t)$ and $C(t)$ initially increase and then decrease after 2020, with their peak times occurring in November 2025. The peak values are 20,736 for $I(t)+C(t)$, 100,026 for $I(t)$, and 10,710 for $C(t)$. When ν takes other given values, $I(t)+C(t), I(t)$ and $C(t)$ all show a continuous decline after 2020.

The above results indicate that an increase in the transmission rate of acutely infected sheep β_I and the proportion of acutely infected sheep p leads to a significant increase in the total number of infected sheep $I(t)+C(t)$ and the number of chronically infected sheep $C(t)$, while extending the duration of the epidemic. Meanwhile, the number of

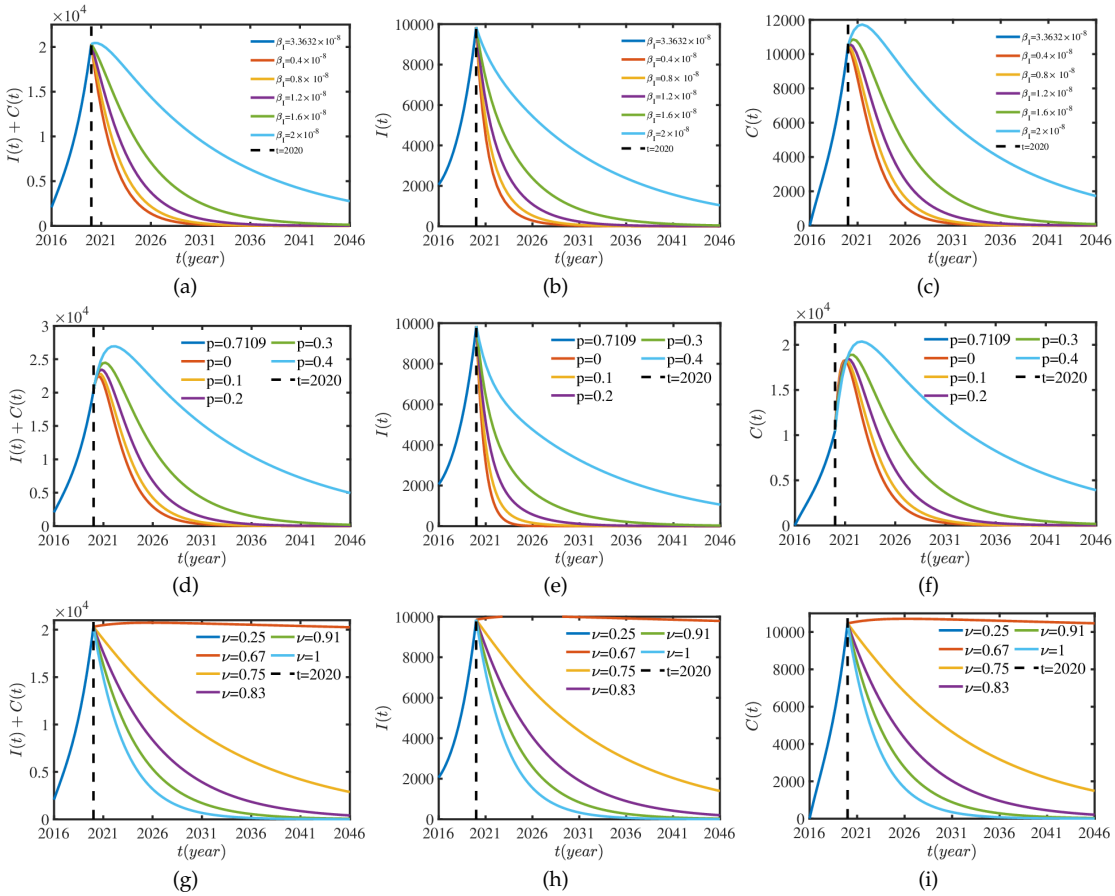

Figure 8: (a) The curves of $I(t)+C(t)$ over time t for different values of β_I. (b) The curves of $I(t)$ over time t for different values of β_I. (c) The curves of $C(t)$ over time t for different values of β_I. (d) The curves of $I(t)+C(t)$ over time t for different values of p. (e) The curves of $I(t)$ over time t for different values of p. (f) The curves of $C(t)$ over time t for different values of p. (g) The curves of $I(t)+C(t)$ over time t for different values of ν. (h) The curves of $I(t)$ over time t for different values of ν. (i) The curves of $C(t)$ over time t for different values of ν.

acutely infected sheep $I(t)$ continuously declines due to rapid transition to chronic infection or removal. The culling rate ν is crucial for controlling the epidemic. A low culling rate is insufficient to curb the spread of the disease, whereas a high culling rate can rapidly reduce the total number of infected sheep. Therefore, reducing β_I and p, setting an appropriate culling rate ν, and continuously managing the chronically infected sheep are key measures to mitigate the long-term impact of the disease.

In light of the insufficient disease control achieved by solely adjusting the transition rate from acute to chronic infected sheep (δ), it is necessary to elucidate the results of combining the strategy with other control strategies. Consequently, starting from the year 2020, we implement several dual control strategies:

(5) decreasing the proportion of acutely infected sheep (p) while reducing the transmission rate of acutely infected sheep (β_I);
(6) decreasing p while increasing the culling rate (ν);
(7) reducing β_I while increasing the transition rate from acute to chronic infected sheep (δ);
(8) decreasing p while increasing δ;
(9) increasing δ while increasing ν;
(10) reducing β_I while increasing ν.

These control strategies further monitor the dynamic changes in the number of infected sheep over time, encompassing the total number of infected sheep $I(t)+C(t)$, the number of acutely infected sheep $I(t)$, and the number of chronically infected sheep $C(t)$. This approach aims to assess the impact of various dual control strategies on the progression of the epidemic. The results corresponding to strategies (5)–(10) are respectively illustrated in Figs. 9–14.

By comparing Figs. 9(a)-9(c) and 11(a)-11(c) with Figs. 8(a)-8(c) and 8(g)-8(i), it is found that reducing β_I (increasing ν) while reducing p can advance the peak times of $I(t)+C(t)$ and $C(t)$, but the peak value of $I(t)+C(t)$ remains almost unchanged, while the peak value of $C(t)$ increases significantly. By comparing Figs. 10(a)-10(c) and 12(a)-12(c) with Figs. 8(a)-8(c) and 8(d)-8(f), it is found that reducing β_I (or p) while increasing δ has no significant effect on the peak value and peak time of $I(t)+C(t)$, but it leads to a significant increase in $C(t)$ in the short term. By comparing Figs. 13(a)-(c) with Figs. 8(g)-8(i), it is found that increasing ν and δ simultaneously has little effect on the peak value of $I(t)+C(t)$, but it shortens the peak time and significantly reduces the epidemic duration. It is worth noting that the increase in δ causes a significant increase in $C(t)$ in the short term. By comparing Figs. 11(a)-11(c) and Figs. 14(a)-14(c) with Figs. 8(a)-8(c) and 8(d)-8(f), it is found that reducing β_I (or p) while increasing ν advances the peak times of $I(t)+C(t)$ and $C(t)$ and significantly shortens the epidemic duration. By comparing Figs. 8-14, it is evident that reducing β_I while increasing ν constitutes the optimal control strategy. In this scenario, $I(t)+C(t)$ and $C(t)$ do not exhibit peaks, continuously declining after the implementation of strategies, significantly shortening the epidemic duration.

In Fig. 15, we simultaneously implement three strategies: reducing β_I and p while increasing ν. Comparing with Fig. 14, it can be observed that increasing p has minimal impact on the epidemic duration. However, when $p=0.3,0.4$, the curve of $C(t)$ shows an upward trend initially after the implementation of strategies. Therefore, the optimal control strategy remains reducing β_I while increasing ν.

8 Conclusion and discussion

In this paper, we develop a sheep brucellosis transmission model incorporating acute and chronic infections, two bilinear incidence rates, a saturated incidence rate, and a time

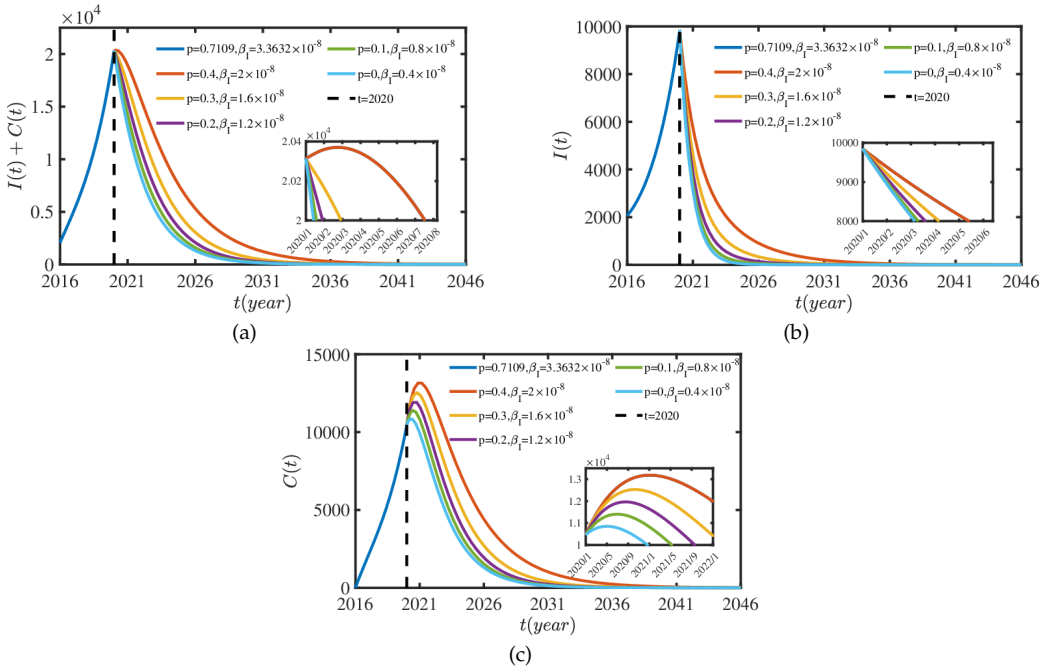

Figure 9: (a) The curves of $I(t)+C(t)$ over time t for different values of p and β_I. (b) The curves of $I(t)$ over time t for different values of p and β_I. (c) The curves of $C(t)$ over time t for different values of p and β_I.

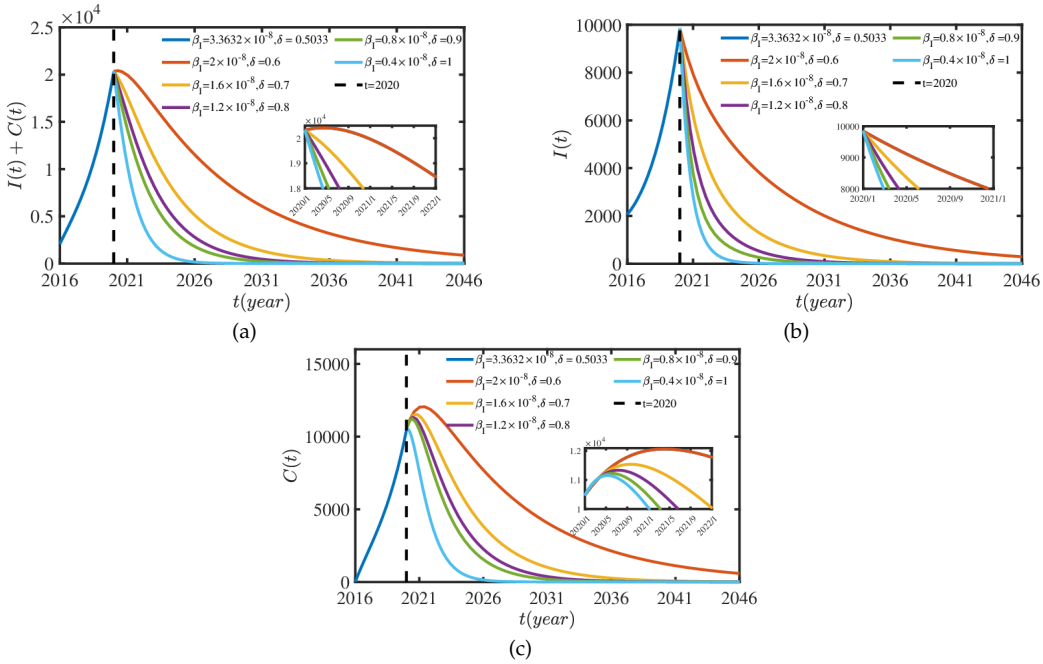

Figure 10: (a) The curves of $I(t)+C(t)$ over time t for different values of β_I and δ. (b) The curves of $I(t)$ over time t for different values of β_I and δ. (c) The curves of $C(t)$ over time t for different values of β_I and δ.

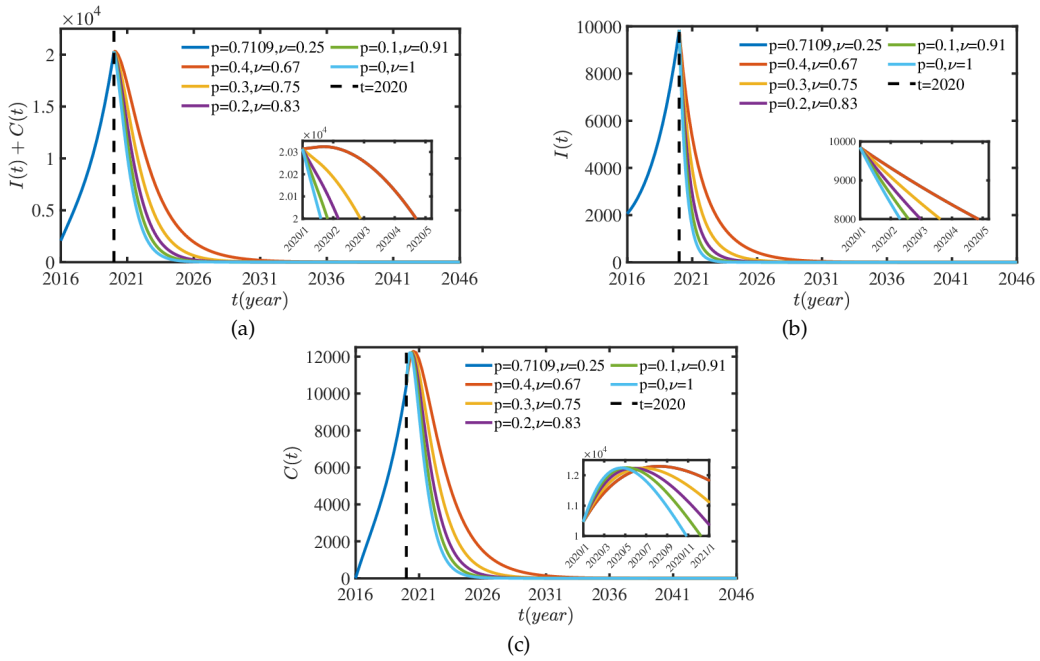

Figure 11: (a) The curves of $I(t)+C(t)$ over time t for different values of p and ν. (b) The curves of $I(t)$ over time t for different values of p and ν. (c) The curves of $C(t)$ over time t for different values of p and ν.

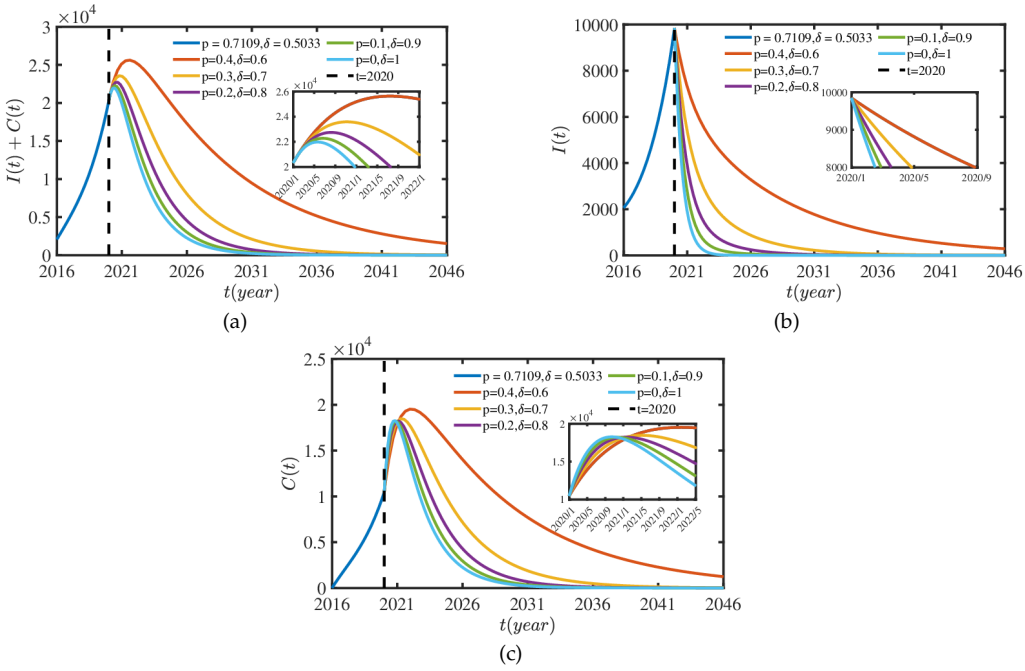

Figure 12: (a) The curves of $I(t)+C(t)$ over time t for different values of p and δ. (b) The curves of $I(t)$ over time t for different values of p and δ. (c) The curves of $C(t)$ over time t for different values of p and δ.

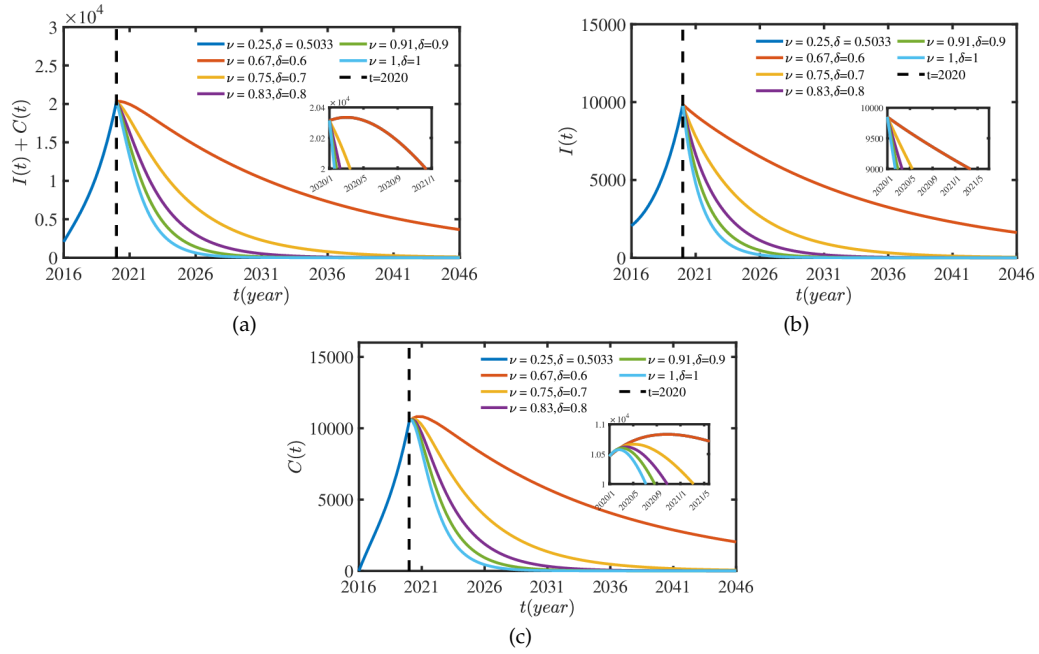

Figure 13: (a) The curves of $I(t)+C(t)$ over time t for different values of δ and ν. (b) The curves of $I(t)$ over time t for different values of δ and ν. (c) The curves of $C(t)$ over time t for different values of δ and ν.

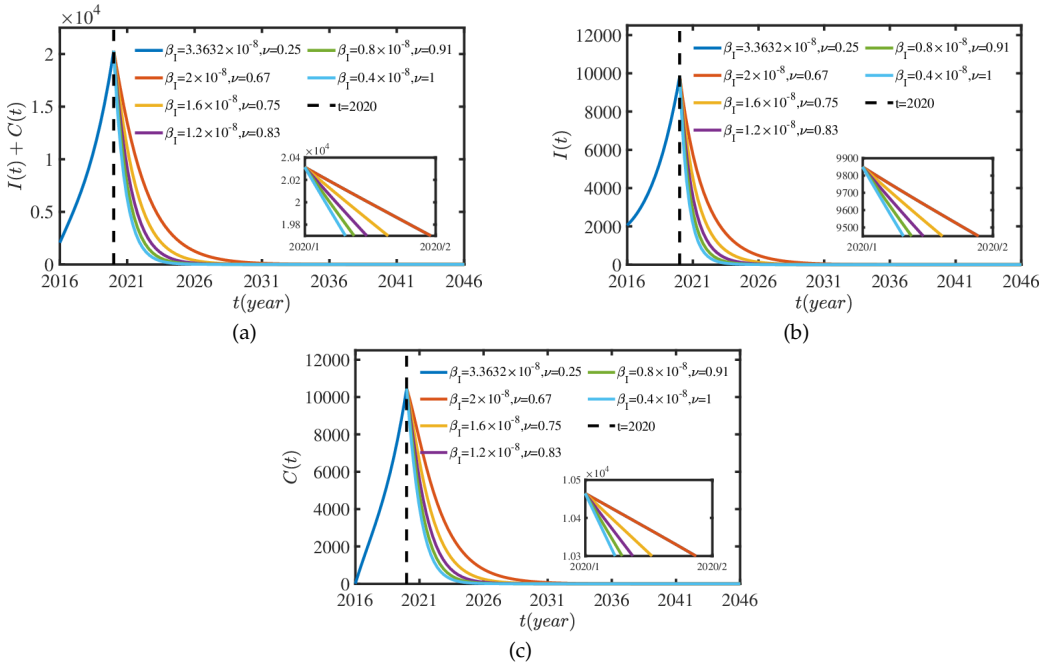

Figure 14: (a) The curves of $I(t)+C(t)$ over time t for different values of β_I and ν. (b) The curves of $I(t)$ over time t for different values of β_I and ν. (c) The curves of $C(t)$ over time t for different values of β_I and ν.

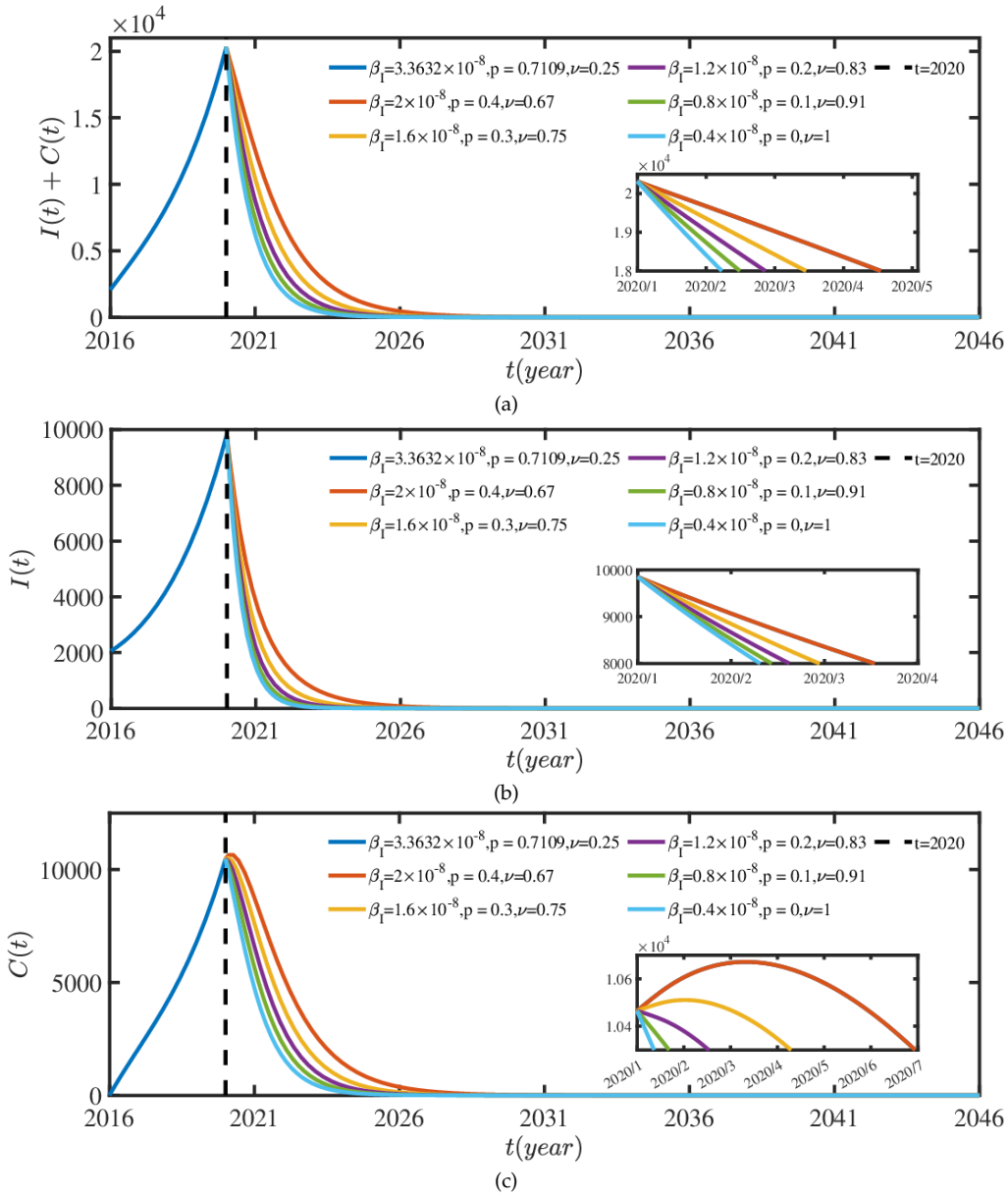

Figure 15: (a) The curves of $I(t)+C(t)$ over time t for different values of β_I,p and ν. (b) The curves of $I(t)$ over time t for different values of β_I,p and ν. (c) The curves of $C(t)$ over time t for different values of β_I,p and ν.

delay. Through theoretical analysis, we have concluded the following: when the basic reproduction number $\mathcal{R}_0 < 1$, the disease-free equilibrium of system (2.3) is globally asymptotically stable; whereas when $\mathcal{R}_0 > 1$, the endemic equilibrium of system (2.3) is globally asymptotically stable.

To verify the applicability of the model, we fit the data of brucellosis cases in sheep in Inner Mongolia from 2016 to 2020 (see Fig. 2) and calculate the basic reproduction number $\mathcal{R}_0 = 1.544$. As shown in Table 2, $\mathcal{R}_{0SI}$ is greater than $\mathcal{R}_{0SC}$, and both are significantly higher than $\mathcal{R}_{0SIB}$ and $\mathcal{R}_{0SCB}$. This indicates that acutely infected sheep play a crucial role in the transmission of brucellosis, thus highlighting the necessity of strengthening prevention and control measures for acutely infected sheep. Meanwhile, the role of chronically infected sheep in the transmission of brucellosis should not be overlooked.

The results of the global sensitivity analysis (PRCC) (see Fig. 3) reveal that the infection rate of acutely infected sheep β_I, the proportion of acutely infected sheep p, the transition rate from acute to chronic infected sheep δ, and the surveillance culling rate ν are key factors influencing the spread of the disease. By conducting local sensitivity analysis on these four parameters (see Figs. 4 and 5), we can obtain the values of $\mathcal{R}_0, \mathcal{R}_{0SC}$ under different values of these parameters. Further, as illustrated in Figs. 6 and 7, reducing β_I, p or increasing ν, can lead to $\mathcal{R}_0 < 1$ and $I^* + C^* = 0$. This provides a theoretical basis for establishing standards to control the spread of the disease.

To further evaluate the impact of different control strategies on disease transmission, we implement single (see Fig. 8) and combined control strategies (see Figs. 9-15) starting from 2020 and observe the changes in the number of total infected sheep, acutely infected sheep, and chronically infected sheep over time. The results show that reducing β_I while increasing ν is the most effective control strategy, significantly shortening the duration of the epidemic. However, reducing p and increasing δ may lead to a significant increase in the number of chronically infected sheep in the initial stage of implementing the strategies, posing challenges to disease control.

Although this paper has already considered the different clinical symptoms of sheep after being infected and the saturated incidence rate of environmental transmission of Brucella, it has not taken into account the effects of spatial heterogeneity, seasonality, and other factors on brucellosis transmission. For instance, the study [22] showed that increasing the random walk rate can effectively prevent local disease spread. Yang *et al.* [43] combined post-infection age with spatial diffusion and found that temporal heterogeneity enhances the oscillation magnitudes of animal populations and Brucella. Ma and Sun [25] revealed that the interaction between periodic fluctuations in survival time and sheep shearing practices is a key factor to periodic disease outbreaks. These studies indicate that taking these factors into account is essential for the study of disease transmission dynamics. In future work, we will further investigate the impact of these factors on brucellosis transmission to refine the model and provide a more scientific basis for disease control.

Acknowledgments

The authors wish to thank the Editor and anonymous reviewers for their insightful comments and suggestions that greatly improved the presentation of this work.

This work was supported by the National Natural Science Foundation of China (Grant Nos. 12271317 and 11871316).

References

[1] B. Aïnseba, C. Benosman, and P. Magal, *A model for ovine brucellosis incorporating direct and indirect transmission*, J. Biol. Dyn., 4(1):2–11, 2010.
[2] A. H. Al-Talafhah, S. Q. Lafi, and Y. Al-Tarazi, *Epidemiology of ovine brucellosis in Awassi sheep in Northern Jordan*, Prev. Vet. Med., 60(4):297–306, 2003.
[3] R. Bagheri Nejad, R. C. Krecek, O. H. Khalaf, N. Hailat, and A. M. Arenas-Gamboa, *Brucellosis in the Middle East: Current situation and a pathway forward*, PLoS Negl. Trop. Dis., 14(5):e0008071, 2020.
[4] M. L. Boschiroli, V. Foulongne, and D. O'Callaghan, *Brucellosis: A worldwide zoonosis*, Curr. Opin. Microbiol., 4(1):58–64, 2001.
[5] D. Bruce, *Note on the discovery of a microorganism in Malta fever*, The Practitioner, 39:161–170, 1887.
[6] B. Buonomo, R. Della Marca, A. d'Onofrio, and M. Groppi, *A behavioural modelling approach to assess the impact of COVID-19 vaccine hesitancy*, J. Theor. Biol., 534:110973, 2022.
[7] China Animal Disease Prevention and Control Center, *Notice on the Issuance of the "2025 National Animal Disease Immunization Technical Guidelines"*, Guangdong Association of Animal Husbandry and Veterinary Medicine, 2025. `https://www.cvma.org.cn/6849/202502/67963.html`
[8] Chinese Veterinary Medical Association, *Epidemiological situation of major animal diseases in China for December 2024*, Chinese Veterinary Medical Association, 2025. `https://www.cvma.org.cn/6849/202502/67963.html`
[9] A. Dénes and A. B. Gumel, *Modeling the impact of quarantine during an outbreak of Ebola virus disease*, Infect. Dis. Model., 4:12–27, 2019.
[10] J. Deng, S. Tang, and H. Shu, *Joint impacts of media, vaccination and treatment on an epidemic Filippov model with application to COVID-19*, J. Theor. Biol., 532(110):698, 2021.
[11] P. H. Elzer, S. D. Hagius, D. S. Davis, V. G. DelVecchio, and F. M. Enright, *Characterization of the caprine model for ruminant brucellosis*, Vet. Microbiol., 90(1-4):425–431, 2002.
[12] G. T. Fosgate, T. E. Carpenter, B. B. Chomel, J. T. Case, E. E. DeBess, and K. F. Reilly, *Time-space clustering of human brucellosis, California, 1973-1992*, Emerg. Infect. Dis., 8(7):672–678, 2002.
[13] J. González-Guzmán and R. Naulin, *Analysis of a model of bovine brucellosis using singular perturbations*, J. Math. Biol., 33(2):211–223, 1994.
[14] Guangdong Association of Animal Husbandry and Veterinary Medicine, *Prevention and control remain tight, objectives more explicit: Analysis of the five-year action plan for brucellosis prevention and control in various regions*, Guangdong Association of Animal Husbandry and Veterinary Medicine, 2022. `https://www.gdaav.org/mobile/article/14204.html`
[15] J. R. Haddock and J. Terjéki, *Liapunov-Razumikhin functions and an invariance principle for functional differential equations*, J. Differential Equations, 48(1):95–122, 1983.
[16] J. K. Hale, *Theory of Functional Differential Equations*, Springer, 1976.
[17] Q. Hou, X. Sun, J. Zhang,Y. Liu, Y. Wang, and Z. Jin, *Modeling the transmission dynamics of sheep brucellosis in Inner Mongolia Autonomous Region, China*, Math. Biosci., 242(1):51–58, 2013.

[18] Q. Hou and F. Zhang, *Global dynamics of a general brucellosis model with discrete delay*, J. Appl. Anal. Comput., 6(1):227–241, 2016.
[19] Inner Mongolia Bureau of Statistics, *2015–2021 Inner Mongolia Bureau of Statistics Yearbook*, China Statistics, 2022. https://tj.nmg.gov.cn/datashow/pubmgr/publishmanage.htm?m=queryPubData&procode=0003&cmenu=A017
[20] M. Li, X. Pei, J. Zhang, and L. Li, *Asymptotic analysis of endemic equilibrium to a brucellosis model*, Math. Biosci. Eng., 16(5):5836–5850, 2019.
[21] M. Li, G. Sun, J. Zhang, Z. Jin, X. Sun, Y. Wang, B. Huang, and Y. Zheng, *Transmission dynamics and control for a brucellosis model in Hinggan League of Inner Mongolia, China*, Math. Biosci. Eng., 11(5):1115–1137, 2014.
[22] S. Liu, Z. Bai, and G. Sun, *Global dynamics of a reaction-diffusion brucellosis model with spatiotemporal heterogeneity and nonlocal delay*, Nonlinearity, 36(11):5699, 2023.
[23] S. Liu, J. Hu, Y. Zhao, X. Wang, and X. Wang, *Prediction and control for the transmission of brucellosis in inner Mongolia, China*, Sci. Rep., 15(1):3532, 2025.
[24] X. Ma, M. Li, J. Zhang, X. Luo, and G.-Q. Sun, *Interactions of periodic birth and shearing induce outbreak of brucellosis in Inner Mongolia*, Int. J. Biomath., 15(8):2250043, 2022.
[25] X. Ma and G. Sun, *Global dynamics of a periodic brucellosis model with time delay and environmental factors*, Appl. Math. Model., 130:288–309, 2024.
[26] S. Marino, I. B. Hogue, C. J. Ray, and D. E. Kirschner, *A methodology for performing global uncertainty and sensitivity analysis in systems biology*, J. Theor. Biol., 254(1):178–196, 2008.
[27] A. Minas, M. Minas, A. Stournara, and S. Tselepidis, *The "effects" of Rev-1 vaccination of sheep and goats on human brucellosis in Greece*, Prev. Vet. Med., 64(1):41–47, 2004.
[28] Ministry of Agriculture and Rural Affairs of the People's Republic of China, *Veterinary Bulletin (2016/2-2021/1)*, Beijing: Ministry of Agriculture and Rural Affairs of the People's Republic of China, 2016-2021. https://www.moa.gov.cn/gk/sygb/
[29] G. Pappas, N. Akritidis, M. Bosilkovski, and E. Tsianos, *Brucellosis*, N. Engl. J. Med., 352(22):2325–2336, 2005.
[30] G. Pappas, P. Papadimitriou, N. Akritidis, L. Christou, and E. V. Tsianos, *The new global map of human brucellosis*, Lancet Infect. Dis., 6(2):91–99, 2006.
[31] X. Pei, X.-L. Wu, P. Pei, M.-T. Li, J. Zhang, and X.-X. Zhan, *Dynamic modeling and analysis of brucellosis on metapopulation network: Heilongjiang as cases*, Chinese Phys. B, 34(1):018904, 2024.
[32] Y. Qin, X. Pei, M. Li, and Y. Chai, *Transmission dynamics of brucellosis with patch model: Shanxi and Hebei Provinces as cases*, Math. Biosci. Eng., 19(6):6396–6414, 2022.
[33] K. A. Qureshi et al., *Brucellosis: Epidemiology, pathogenesis, diagnosis and treatment – a comprehensive review*, Ann. Med., 55(2):2295398, 2023.
[34] M. Refai, *Incidence and control of brucellosis in the Near East region*, Vet. Microbiol., 90(1-4):81–110, 2002.
[35] H. Ren and R. Xu, *Prevention and control of Ebola virus transmission: Mathematical modelling and data fitting*, J. Math. Biol., 89(2):25, 2024.
[36] S. Roy, T. F. McElwain, and Y. Wan, *A network control theory approach to modeling and optimal control of zoonoses: Case study of brucellosis transmission in sub-Saharan Africa*, PLoS Negl. Trop. Dis., 5(10):e1259, 2011.
[37] C. Song, R. Xu, N. Bai, X. H. Tian, and J. Z. Lin, *Global dynamics and optimal control of a cholera transmission model with vaccination strategy and multiple pathways*, Math. Biosci. Eng., 17(4):4210–4224, 2020.
[38] K. Song, Y. Zhang, R. Sun, M. Guo, D. Han, L. Ren, and L. Shu, *Bibliometric analysis of brucel-*

losis by CiteSpace, J. Pharm. Pract. Serv., 41(5):310–315, 2023.
[39] M. Ussain, *Understanding brucellosis in sheep: Causes, symptoms, prevention, and management*, J. Vet. Med. Surg., 7(3):29, 2023.
[40] L.-S. Wang, M.-T. Li, X. Pei, J. Zhang, G.-Q. Sun, and Z. Jin, *Cost assessment of optimal control strategy for brucellosis dynamic model based on economic factors*, Commun. Nonlinear Sci. Numer. Simul., 124:107310, 2023.
[41] World Health Organization, *Brucellosis in humans and animals*, 2006. `https://www.who.int/publications/i/item/9789241547130`
[42] World Health Organization, *Brucellosis*, 2020. `https://www.who.int/news-room/fact-sheets/detail/brucellosis`
[43] J. Yang, R. Xu, and J. Li, *Threshold dynamics of an age-space structured brucellosis disease model with Neumann boundary condition*, Nonlinear Anal. Real World Appl., 50:192–217, 2019.
[44] J. Yang, R. Xu, and H. Sun, *Dynamics of a seasonal brucellosis disease model with nonlocal transmission and spatial diffusion*, Commun. Nonlinear Sci. Numer. Simul., 94:105551, 2021.
[45] L. Yang, M. Fan, and Y. Wang, *Dynamic modeling of prevention and control of brucellosis in China: A systematic review*, Transbound. Emerg. Dis., 2025:1393722, 2025.
[46] J. Zhang, Z. Jin, L. Li, and X.-D. Sun, *Cost assessment of control measure for brucellosis in Jilin province, China*, Chaos Solit. Fractals, 104:798–805, 2017.
[47] J. Zhang, G.-Q. Sun, X.-D. Sun, Q. Hou, M. Li, B. Huang, H. Wang, and Z. Jin, *Prediction and control of brucellosis transmission of dairy cattle in Zhejiang Province, China*, PLoS One, 9(11):e108592, 2014.
[48] W. Zhang, J. Zhang, Y.-P. Wu, and L. Li, *Dynamical analysis of the SEIB model for brucellosis transmission to the dairy cows with immunological threshold*, Complexity, 2019:1–13, 2019.
[49] Z. Zhang, X. Ma, Y. Zhang, G. Sun, and Z.-K. Zhang, *Identifying critical driving factors for human brucellosis in Inner Mongolia, China*, Phys. A, 626:129073, 2023.
[50] Z. Zhang, J. Zhang, L. Li, Z. Guo, Z.-K. Zhang, and G.-Q. Sun, *Quantifying the effectiveness of brucellosis control strategies in northern China using a mechanistic and data-driven model*, Chaos Solit. Fractals, 185:115121, 2024.
[51] X.-Q. Zhao, *Dynamical Systems in Population Biology*, in: CMS Books in Mathematics, Springer, 2017.
[52] X.-Q. Zhao, *The linear stability and basic reproduction numbers for autonomous FDEs*, Discrete Contin. Dyn. Syst. Ser. S, 17:708–719, 2024.
[53] Y. Zhao, D. Pan, Y. Zhang, L. Ma, H. Li, J. Li, S. Liu, and P. Liang, *Spatial interpolation and spatiotemporal scanning analysis of human brucellosis in mainland China from 2012 to 2018*, Sci. Rep., 15(1):7403, 2025.
[54] L. Zhou, M. Fan, Q. Hou, Z. Jin, and X. Sun, *Transmission dynamics and optimal control of brucellosis in Inner Mongolia of China*, Math. Biosci. Eng., 15(2):543–567, 2018.
[55] J. Zinsstag, F. Roth, D. Orkhon, G. Chimed-Ochir, M. Nansalmaa, J. Kolar, and P. Vounatsou, *A model of animal-human brucellosis transmission in Mongolia*, Prev. Vet. Med., 69(1-2):77–95, 2005.